Running Title: DNA repair dysfunction and PARPi in lobular breast cancer

Research article

Co-regulator activity of Mediator of DNA Damage Checkpoint 1 (MDC1) is associated with DNA repair dysfunction and PARP inhibitor sensitivity in lobular carcinoma of the breast

Joseph L. Sottnik[1], Madeleine T. Shackleford[1], Camryn S. Nesiba[1], Amanda L. Richer[2,3], Jordan M. Swartz[1], Carmen E. Rowland[1], Maggie Musick[1], Rui Fu[2,3], Patricia L. Opresko[5], Sanjana Mehrotra[1], Jay R. Hesselberth[2,3], Jennifer R. Diamond[5], Matthew J. Sikora[1,3]

Affiliations

[1]Dept. of Pathology, University of Colorado Anschutz Medical Campus
[2]Dept. of Biochemistry and Molecular Genetics, University of Colorado Anschutz Medical Campus
[3]RNA Bioscience Initiative, University of Colorado School of Medicine
[4]UPMC Hillman Cancer Center; University of Pittsburgh School of Medicine
[5]Dept. of Medical Oncology, University of Colorado Anschutz Medical Campus

Corresponding author

Matthew J. Sikora, PhD.; Mail Stop 8104, Research Complex 1 South, Room 5110, 12801 E. 17th Ave.; Aurora, CO 80045. Tel: (303)724-4301; Fax: (303)724-3712; email: matthew.sikora@cuanschutz.edu. Twitter: @mjsikora

Authors' contributions

MJS conceived of the project and experiments. JLS, MTS, ALR, CSN, RF, SM, and MJS designed and performed experiments and data analyses. JLS and CSN developed models for the project. All authors contributed to data analysis and interpretation. MJS wrote the draft manuscript; all authors read and revised the manuscript and have read and approved of this version of the manuscript.

Funding

This work was supported by ACS RSG-20-042-01-DMC from the American Cancer Society (MJS), R01 CA251621 from the National Institutes of Health (MJS), grants from the Cancer League of Colorado, Inc (MJS), support from the Dynami Foundation (MJS), the Lobular Breast Cancer Research Fund at CU Anschutz (MJS), support from the Women's Cancer Developmental Therapeutics Program at CU Anschutz (JRD and MJS), and a grant from the RNA Bioscience Initiative at the CU Anschutz School of Medicine (MJS and JRH). This work utilized the U. Colorado Cancer Center Genomics Shared Resource, Biostatistics and Bioinformatics Shared Resource, Cell Technologies Shared Resource (RRID: SCR_021982), Research Histology (RRID: SCR_021994), and Flow Cytometry Shared Resource (RRID: SCR_022035) supported by P30 CA046934. The content of this manuscript is solely the responsibility of the authors and does not necessarily represent the official views of the National Institutes of Health or other agencies.

Key words

Invasive lobular carcinoma, breast cancer, MDC1, estrogen receptor, DNA repair, DNA damage response, PARP inhibitors.

ABSTRACT

Invasive lobular carcinoma of the breast (ILC) are typically estrogen receptor α (ER)-positive and present with biomarkers of anti-estrogen sensitive disease, yet patients with ILC face uniquely poor long-term outcomes with increased recurrence risk, suggesting endocrine response and ER function are unique in ILC. We previously found specifically in ILC cells that ER is co-regulated by the DNA repair protein Mediator of DNA Damage Checkpoint 1 (MDC1). This novel MDC1 activity, however, was associated with dysfunction in the canonical DNA repair activity of MDC1, but absent typical features of DNA repair deficiency. To understand reciprocal activities of MDC1, we profiled the MDC1 interactome and found MDC1-associated proteins in ILC cells mirror a "BRCA-like" state lacking key homologous recombination (HR) proteins, consistent with HR dysfunction but distinct from classic "BRCAness". HR dysfunction in ILC cells was mirrored in single-cell transcriptome and DNA repair activity analyses, along with DNA repair signaling and functional data, showing dysfunctional HR induction and resolution. In parallel, ILC tumor data are consistent with a distinct form of HR dysfunction via impaired HR resolution, lacking BRCA-like genomic scarring but with elevated signatures of PARP inhibitor sensitivity. We tested whether this HR dysfunction could indeed be exploited using PARP inhibition and found that talazoparib treatment produced a durable growth suppression *in vitro* and in multiple ILC xenografts *in vivo*. ILC-specific ER:MDC1 activity creates a new context for ER and MDC1 function in ILC, at the cost of a DNA repair dysfunction that is therapeutically targetable.

Significance: ILC are rarely associated with biomarkers of HR deficiency, and as such patients are rarely eligible for treatment with PARP inhibitors. Our work suggests ILC present with a previously unappreciated form of HR dysfunction, linked to ILC-specific genomic activity of ER and MDC1, which imparts sensitivity to PARP inhibition.

INTRODUCTION

Invasive lobular carcinoma of the breast (ILC) is increasingly recognized as a distinct clinical and molecular entity among breast cancers [1–3]. Beyond ILC's unique histopathological presentation – i.e., infiltrating the breast in a discohesive, "single-file" pattern – we now appreciate that ILC have distinct genetic and cellular features relative to breast cancers of no special type (also known as invasive ductal carcinoma, IDC). Most ILC present with biomarkers of low-risk disease, as ~95% are estrogen receptor α (ER)-positive and ~80% are classified as the Luminal A molecular subtype [4], but retrospective studies suggest that ILC carry more long-term risk of poor outcomes than IDC. Retrospective studies have shown that 5-8 years after diagnosis, ILC recurrences increase relative to IDC regardless of ER status, with ER+ ILC having a ~30% increased risk of recurrence vs ER+ IDC [5–8]. Further, recurrent or metastatic ILC presents distinct challenges, as ILC are unique among breast cancers in metastasizing to the GI/GU, peritoneum, ovary/uterus, the orbit, and the leptomeninges [2,5,9,10]. Treating ILC is further complicated due to controversies related to anti-estrogen resistance [11], the limited benefit of chemotherapy for most patients with ILC [2,12,13], and the lack of any approved precision or targeted treatments designed for ILC. New treatments for patients with ILC are needed, but strategies must be driven by advances in defining the unique biology of ILC.

We previously profiled the ER interactome in ILC cells with the goal of defining novel ER co-regulators that mediate ILC-specific endocrine response or anti-estrogen resistance [14]. This approach identified Mediator of DNA Damage Checkpoint 1 (MDC1) as a critical ER co-regulator specifically in ILC cells. We found that the ER:MDC1 interaction is likely unique to ILC cells, that MDC1 was specifically required for ER-driven growth in ILC but not IDC cells, and that MDC1 knockdown broadly dysregulated the ER transcriptome in ILC cells. As MDC1 has no known enzymatic activity, the mechanism by which MDC1 co-regulates ER is unknown. The canonical role of MDC1, however, is to bind new phospho-H2AX (γH2AX) marks at DNA double-strand breaks and scaffold double-strand break repair machinery, including the MRE11/RAD50/NBS1 (MRN) complex and additional downstream partners that ultimately facilitate repair [15–17]. The MDC1 scaffold initiates signaling via CHK1/2 to cause cell cycle arrest, and coordinates DNA double-strand break repair either via homologous recombination (HR) or non-homologous end joining (NHEJ). While we confirmed these canonical DNA repair roles of MDC1 in IDC cells, this was not the case in ILC cells. For example, γH2AX foci formation, which requires MDC1 [18], was limited in ILC cells and γH2AX instead presented largely as an elevated pan-nuclear signal; pan-nuclear γH2AX has been linked to DNA repair dysfunction [19]. These observations collectively suggest that the novel ER co-regulator activity of MDC1 may come at a cost of compromised MDC1 activity in DNA repair.

ILC do not typically present with biomarkers of overt DNA repair deficiency such as germline *BRCA1/2* mutations. These mutations are uncommon in ILC and are depleted relative to IDC; ILC accounts for up to 15% of all breast cancers, but only ~2% and ~8% of breast cancers in *BRCA1* or *BRCA2* mutation carriers, respectively, and germline *PALB2* and *TP53* mutations are also rare in ILC [20–22]. Similarly, somatic mutations in genes associated with DNA repair are uncommon in primary ILC, e.g. somatic *TP53* mutations were found in only ~8% of ILC, and only 5.7% of Luminal A ILC, in the Cancer Genome Atlas (TCGA)[4]. ILC genomes are typically considered 'quiet' and overall show fewer structural re-arrangements than other breast cancers. Similarly, HR deficiency as defined by various mutational signatures is not common in ILC but is typically associated with the few ILC that are *TP53*-mutant or with germline *BRCA1/2* mutations [3].

Together these observations would suggest that DNA repair deficiency is uncommon in ILC. However, data from TCGA show that a putative transcriptional subtype of ILC, "Proliferative" ILC, was associated with an elevated DNA damage response (DDR) signature in protein array analyses [4]. This is paralleled by the identification of frequent *MDM4* amplification in ILC tumors (17%) [23]. MDM4 was required for proliferation and survival of *TP53*-wild type ILC cell lines, as such, suppression of p53-driven pathways by mechanisms independent of *TP53* mutation may be an underappreciated feature of ILC. Additionally, in Foundation Medicine data, primary ILC were shown to have increased tumor mutational burden relative to IDC, which further progressed with metastatic ILC [24]. Among metastatic ER+ breast cancers, 8.9% of ILC were TMB-high or extreme versus 1.5% of IDC (p=0.0016); ~37% of ILC were classified as TMB-medium or higher versus only 25% of IDC (p=0.013) [24]. Collectively these data suggest that our understanding of DNA repair signaling and function in ILC is incomplete, and may not be adequately defined as 'proficient' versus 'deficient', as it relates to *BRCA1/2* mutant tumors.

Based on the novel ER:MDC1 interaction in ILC cells and putative link to DNA repair dysfunction, we hypothesized that profiling the MDC1 interactome in ILC cells would both shed light on mechanisms by which MDC1 acts as an ER co-regulator, and offer insight into DNA repair function in ILC cells. These studies confirmed connections between the co-regulator activity versus DNA repair functions of MDC1, and identified potential mechanistic underpinnings of a "BRCA-like" phenotype in ILC cells. We explored whether MDC1-related "molecular BRCAness" in ILC cells provided opportunities for synthetic lethal therapeutic approaches. Better understanding of the cross-talk linking ER:MDC1, transcriptional regulation, and DNA repair capacity offers unique opportunities to understand ILC biology and develop precision treatments around synthetic vulnerabilities unique to ILC.

RESULTS

The MDC1 interactome in ILC cells indicates DNA damage response dysfunction

We profiled the MDC1 interactome in ILC cells to identify transcriptional co-regulator partners of ER:MDC1, and to assess differential MDC1 association with canonical DNA repair partners, by performing MDC1 co-immunoprecipitation + mass spectrometry (IP/MS) in ILC versus IDC cells. Of note, proteomic approaches have previously shown MDC1 association with the MRN complex and other DNA repair proteins, but studies to date have used exogenous and/or tagged versions of full-length MDC1 or MDC1 fragments, and have only been performed in HeLa, HEK293 (293), or U2OS cells [25–29]. We performed endogenous MDC1 IP using a validated MDC1 antibody from ER+ cell lines MCF7 (IDC), HCC1428 (IDC, *BRCA2*-mutant), MM134 (ILC), and 44PE (ILC), as well as 293FT cells (to compare our approach to literature data). IP/MS was performed absent DNA damaging agents, from biological duplicate MDC1 IP samples and a matched IgG control per cell line; an additional pair of samples for MM134 was treated with the anti-estrogen fulvestrant for 24hrs prior to IP. MS parameters and analyses are described in Material and Methods. MDC1 was strongly enriched in targeted IP versus IgG across all samples (MDC1 iBAQ: ~90-fold up to >1000-fold for MDC1 IP vs IgG, **Supplemental Figure 1A**).

Across all 5 cell lines, over 2000 proteins were enriched relative to IgG controls (**Supplemental File 1**). Identified proteins were most enriched for ribosomal and related mRNA/rRNA-processing proteins (as observed by Salifou et al, discussed below [27]).We excluded/filtered RNA processing proteins to facilitate further analysis (see Methods), yielding n=1666 proteins identified in at least one cell line (**Supplemental File 1**). We first examined MDC1-associated proteins in 293FT cells (n=1497, n=1236 after filtering), and confirmed that the MRN complex (MRE11, RAD50, NBN), constitutive partners of MDC1 in 293FT and other cells, were strongly enriched (**Supplemental Figure 1B**). More broadly, DNA repair pathway proteins were strongly enriched as well as epigenomic proteins, consistent with the functions of epigenomic proteins in DNA repair and reported roles for MDC1 in chromatin remodeling [30] (**Supplemental Figure 1C, Supplemental File 1**).

We compared our 293FT data to MDC1 interactome data from Salifou et al [27], the only other proteome-wide MDC1 interactome data published to date. Whereas we utilized an MDC1-specific antibody for IP, Salifou et al used CRISPR/Cas9 to append a Flag-hemagglutinin (HA) tag to the N-terminus of endogenous MDC1 in 293FT cells, then performed tandem affinity purification of Flag/HA-MDC1, reporting n=384 MDC1 associated proteins (n=276 after filtering as above). As noted above, both datasets were strongly enriched for splicing and translational proteins (**Supplemental Figure 2A**), supporting a role for MDC1 in protecting genomic integrity at actively transcribed sites [27,31]. Upon filtering, our data using direct MDC1 IP was specifically enriched in DNA repair and chromatin remodeling proteins (**Supplemental Figure 2B**). Of note, our data included greater depth of coverage of similar biological pathways compared to the Flag/HA-MDC1 dataset (**Supplemental Figure 2C**), and proteins in pathways enriched only in the Flag/HA-MDC1 dataset were still identified in our data (**Supplemental Figure 2D**). These data support that our direct MDC1 IP with MS confirms prior observations on MDC1 association with mRNA/translational machinery and provides greater representation and enrichment for MDC1-associated DNA repair and chromatin remodeling proteins.

In the breast cancer cell lines, >700 MDC1-associated proteins were identified per cell line after filtering (**Figure 1A**). Hierarchical clustering showed that the MDC1 interactome in ILC cells was distinct from MCF7

(IDC) cells and more closely related to the *BRCA2*-mutant HCC1428 cells (**Figure 1A**), which was consistent with a relative depletion of MDC1-associated DNA repair proteins. DNA repair proteins were enriched overall in all 4 lines (**Supplemental File 1**); however, though NHEJ and nucleotide-excision repair were enriched in ILC cells, HR proteins were enriched only in MCF7 but depleted in the ILC and *BRCA2*-mutant cells (**Figure 1B**). This depletion of HR proteins included minimal/absent MRN complex proteins and other HR factors (**Figure 1C**). Conversely, despite the depletion of DNA damage response (DDR)/HR proteins, the MDC1 interactome in ILC cells was strongly enriched for epigenomic partners (**Figure 1D**), e.g. histone acetylation proteins. Distinct subsets of histone acetylation factors were identified in MCF7/IDC vs ILC (and *BRCA2*-mutant) cells, e.g. RUVBL1/2 in the former and the HBO1-complex (ING5, BRPF3, MEAF6, JADE3) in the latter (**Figure 1E**). Collectively these data suggest that the constitutive association of MRN with MDC1 may not be absolute, and that the absence/depletion of MRN on MDC1 is associated with DNA repair/HR dysfunction. The depletion of MRN and other HR proteins among MDC1-associated proteins in ILC is consistent with the pan-nuclear γH2AX localization we previously reported [14]. However, the epigenomic functions of MDC1 likely remain intact despite DDR dysfunction and thus may be associated with the co-regulator functions of MDC1 in ILC cells.

Inhibiting estrogen receptor in ILC cells restores DDR/HR proteins in the MDC1 interactome

We hypothesized that the novel ER:MDC1 interaction in ILC cells is at least in part responsible for remodeling the MDC1 interactome, and tested this by treating MM134 cells with the ER antagonist and degrader fulvestrant prior to MDC1 IP/MS. Hierarchical clustering showed that with fulvestrant the MDC1 interactome in MM134 more closely resembled MCF7 cells (i.e. HR-competent cells; **Figure 2A**). Strikingly, this change was associated with increased MDC1-association with HR pathway proteins (**Figure 2B**), including the MRN complex, specifically MRE11 and RAD50 (**Figure 2C**). Notably, HR proteins gained in MM134+Fulv versus MM134 (**Figure 2C**, orange bar) were all identified as MDC1-associated in MCF7 cells, suggesting that these MDC1 interactions were restored with fulvestrant treatment, rather than fulvestrant driving new MDC1 interactions. MDC1 association with epigenomic proteins remained enriched in fulvestrant treated cells (**Figure 2D**), but we noted changes in the specific proteins identified. In particular, among histone acetylation proteins, several proteins were shifted by fulvestrant treatment to resemble the state in MCF7 cells, including restoration of RUVBL2 and depletion of HBO1-complex proteins ING5, JADE3, and BRPF3 (**Figure 2E**, orange bar). These observations support that ER plays a role in regulating the cross-talk between genomic functions of MDC1 and the DDR functions of MDC1 at least in part through control over the MDC1 interactome.

Co-regulator activity of MDC1 is linked to specific cellular DNA repair activity

We explored the cross-talk between MDC1 co-regulator activity with ER versus MDC1 DNA repair activity, using a single-cell approach to measure DNA repair called “Haircut”. Haircut profiles DNA repair activities using DNA oligo substrates for specific repair enzymes by including oligonucleotide substrates in the single-cell emulsion. Repair enzymes create nicks in the substrates, and sequencing quantifies repair activities by comparing modified and unmodified oligo substrates. Haircut profiles PARP-related single-strand repair, quantifying the activity of base excision repair and nucleotide excision/incision repair enzymes in a single reaction (See Figures 1-2 and Supplemental Figure 1 in [32], also [33]). We coupled Haircut with targeted transcriptome analysis (10X Genomics Pan-cancer capture panel, n=1,253 genes), allowing us to profile DNA

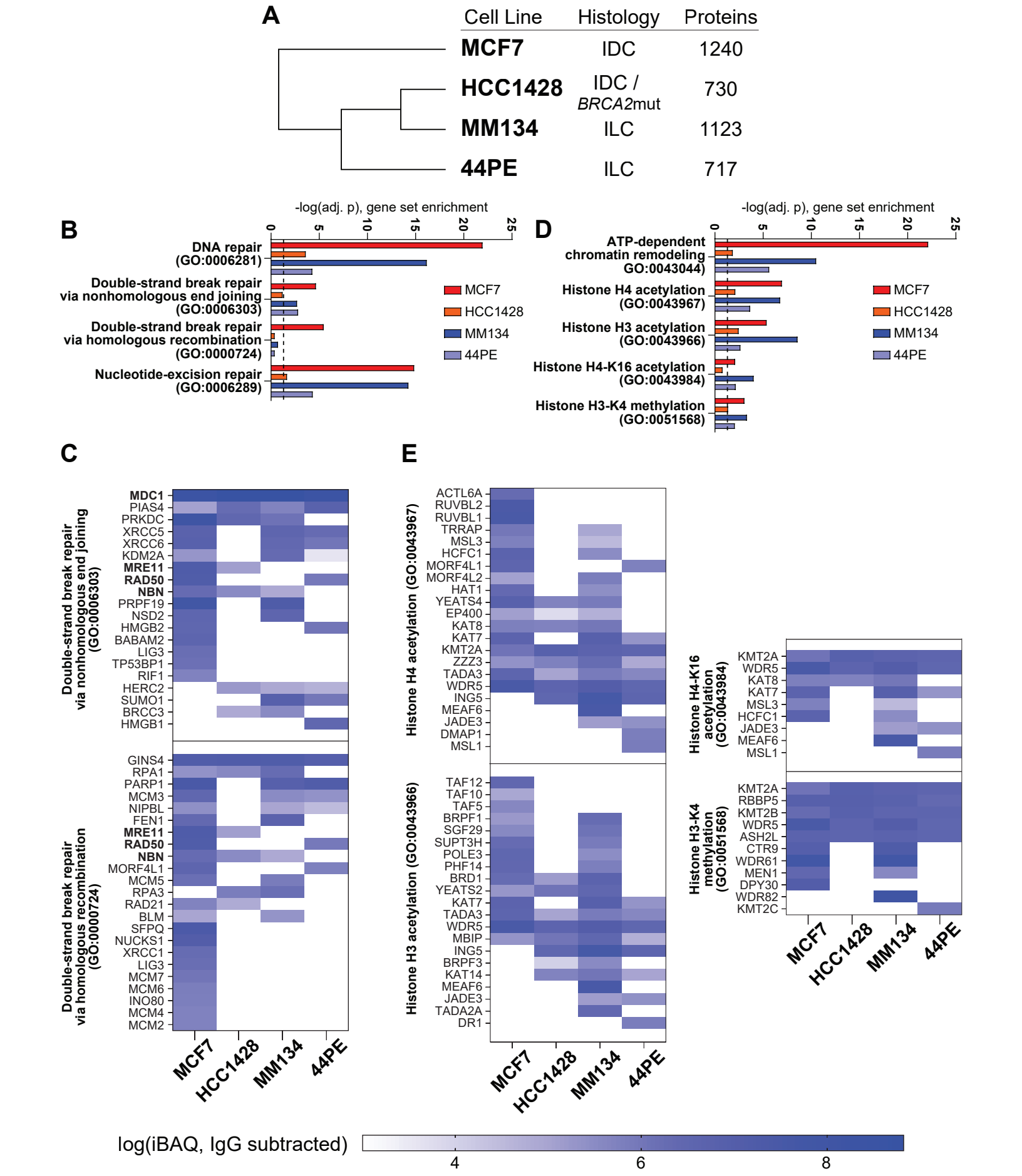

Figure 1. MDC1 interactome in ILC cells mirrors a BRCA-mutant state. (A) Hierarchical clustering (Pearson) of MDC1 associated proteins after filtering of RNA-processing related proteins. **(B,D)** Gene set enrichment against GO Biological Processes. Dashed line: adj. p = 0.05. **(C,E)** Mean IgG-subtracted intensity of duplicate IP/MS samples for proteins in indicated ontology groups.

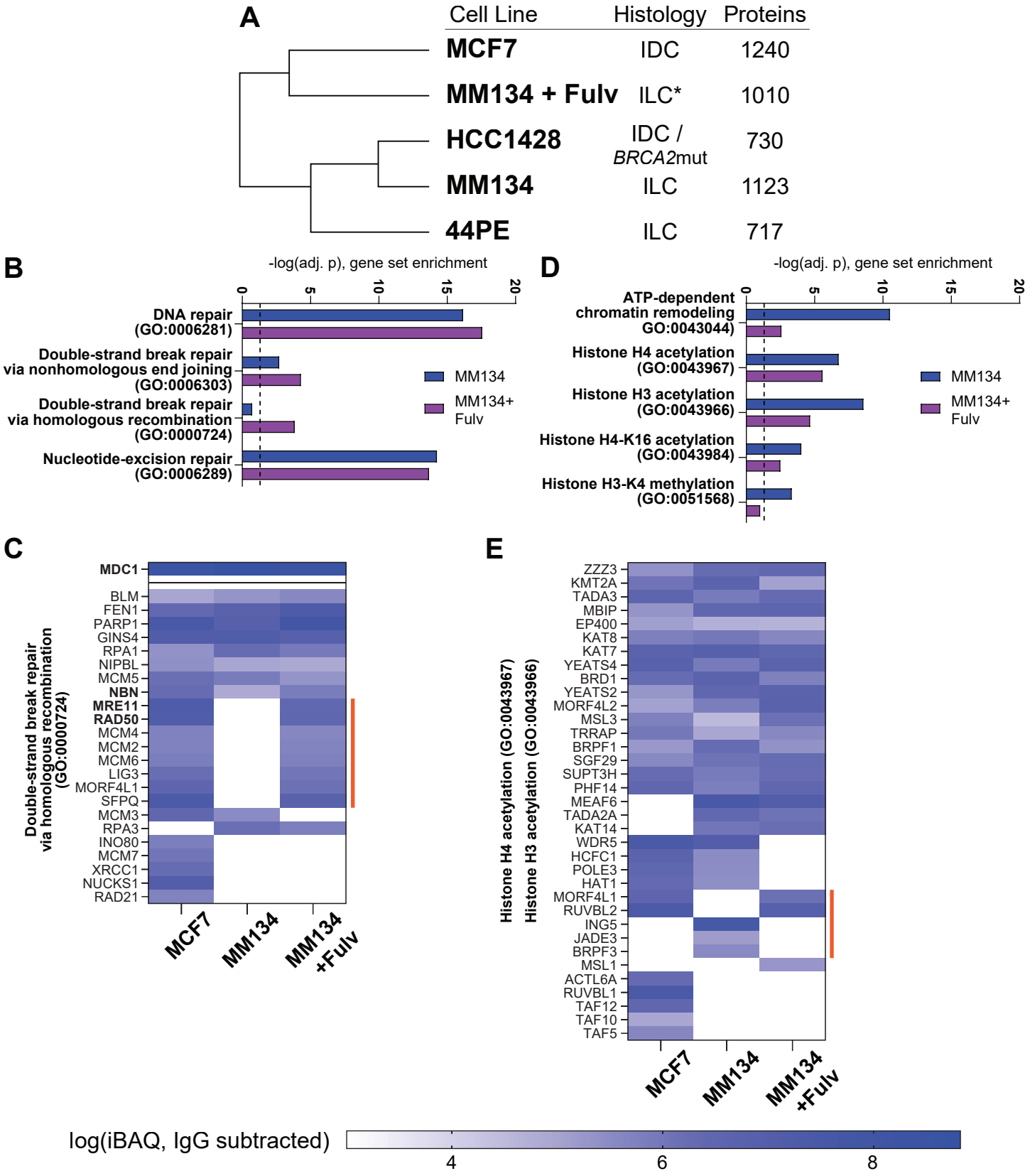

Figure 2. ER inhibition with fulvestrant shifts MDC1 interactome toward a non-BCRA-mutant state. (A) Hierarchical clustering (Pearson) of MDC1 associated proteins as in Figure 1A, with inclusion of MM134+Fulvestrant samples. **(B,D)** Gene set enrichment against GO Biological Processes. Dashed line: adj. p = 0.05. **(C,E)** Mean IgG-subtracted intensity of duplicate IP/MS samples for proteins in indicated ontology groups. Orange bar identifies IP/MS hits putative remodeled by fulvestrant treatment discussed in text.

repair activity and gene expression in individual cells. We performed scRNAseq + Haircut in MM134 ±E2 (n=8,307 cells: –E2, n=4,940; +E2, n=3,367) (**Supplemental File 2** – see access link in methods). We extrapolated ER activity and co-regulator activity (MDC1 vs pioneer factor FOXA1; **Figure 3A**) from the expression of n=259 ER target genes in the capture panel based on our prior RNAseq study [14] (cell cycle genes excluded; **Supplemental File 2**), and examined ER:MDC1 activity versus DNA repair capacities.

Gene expression via the Pan-cancer capture panel defined 8 clusters (**Figure 3B**) with distinct ER and co-regulator activity (**Figure 3C**; **Supplemental Figure 3A**). Two clusters were primarily –E2 cells with minimal activation of ER target genes (Clusters 6 & 2), while other clusters had increasing fractions of +E2 cells and differential activation of ER target genes. In two clusters, ER:MDC1 target genes were active while MDC1-independent ER target genes were inactive (**Figure 3C**, clusters 5 & 7; C5/C7). Paralleling this separate activation of MDC1-dependent vs –independent ER target genes, we noted that activation of MDC1-dependent ER targets was effectively independent of cell cycle, whereas MDC1-independent ER targets were activated in S and G2/M versus G1 independent of E2 (**Supplemental Figure 3B**). Specific activation of ER:MDC1 in C5 and C7 and across cell cycle supports that MDC1 has a distinct role in co-regulating ER relative to other factors, i.e., ER:MDC1 activity is separate from ER:FOXA1 and likely is a functional subset of the ER transcriptome.

Notably, C5/7 largely lacked S-phase cells and were enriched for G1 and G2/M cells (as defined by gene expression), respectively. Despite the enrichment for G2/M cells in C7, both C5/7 expressed markedly low levels of genes associated with HR (**Figure 3D**), similar to the predominantly –E2/G1 phase clusters 6 & 2. C5/7 were similarly distinct in DNA repair capacity in Haircut analysis. The Haircut "Abasic" reporters primarily measure base excision repair (BER) activity of the enzyme APE1, and we found that +E2 cells had lower BER/APE1 activity versus –E2 cells (**Figure 3E**). In contrast, C5/7 showed elevated BER/APE1 activity and had the highest such activity among the +E2 clusters (**Figure 3F**). The ER target gene activity and Haircut data taken together link MDC1 co-regulator activity to distinct DNA repair activity, and a potential reliance on non-HR pathways to maintain genomic integrity. These observations parallel the putative HR dysfunction indicated by the MDC1 interactome in ILC cells.

ILC cells present with dysfunctional initiation and resolution of homologous recombination

The depletion of HR proteins associated with MDC1 in ILC cells, coupled with our prior observation that ILC cells show primarily pan-nuclear γH2AX in response to DNA damage [14], are consistent with DDR or DNA repair dysfunction. However, the nature of this putative dysfunction is unclear. To examine DNA repair signaling further, we induced DNA damage in MM134 (ILC) cells and examined key proteins in DNA damage response (DDR) initiation and resolution. Etoposide treatment led to DDR protein phosphorylation, including those upstream of MDC1 (H2AX, ATM, MRN complex proteins) and downstream of MDC1 (CHK1/2, 53BP1, DNA-PKcs) (**Figure 4A**), supporting that initiation of DDR is intact in these cells. Notably, phosphorylation of NHEJ-associated proteins (53BP1, DNA-PKcs) was rapid and seen within 4hrs, while RAD51 turnover, associated with HR resolution [34,35], was not apparent in MM134 cells. We next examined induction and resolution of DDR protein phosphorylation in MM134 (ILC) compared to MCF7 (IDC) after etoposide treatment. 53BP1 and DNA-PKcs phosphorylation occurred immediately in ILC cells whereas this was delayed in IDC cells (**Figure 4B**), supporting rapid activation of NHEJ in MM134. In parallel, etoposide treatment decreased levels of RAD51 in MCF7, consistent with RAD51 turnover during HR [36], whereas this was not observed in MM134 out to 48hrs post-damage. The lack of RAD51 protein turnover may indicate

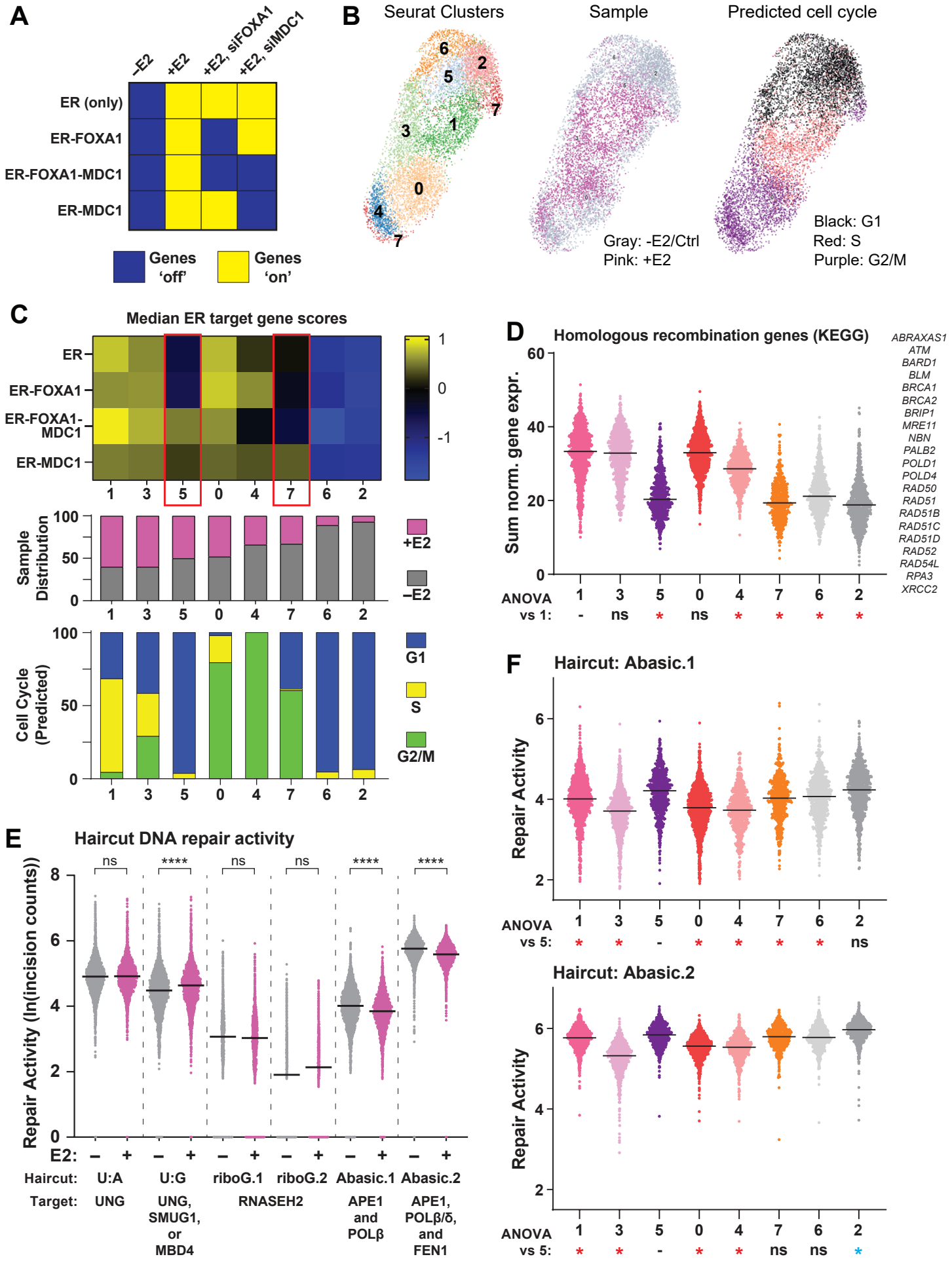

Figure 3. Single cell transcriptome + Haircut data identifies reciprocal MDC1 co-regulator activity versus DNA repair activity. (A) Schematic for predicted ER target gene expression based on dependence on MDC1, FOXA1, or neither factor. Based on RNAseq data from Sottnik & Bordeaux et al, 2021. **(B)** UMAP plot showing Seurat clusters (left), sample/treatment (center), and predicted cell cycle state (right). **(C)** Top, ER target gene scores in each of the 8 Seurat clusters. Single cell scores are a z-score of the relative expression of estrogen-induced and estrogen-repressed genes (see Supplemental File 2). Middle, per cluster fraction of cells from the –E2 vs +E2 samples. Bottom, per cluster distribution of predicted cell cycle state. Points represent individual cells. **(D)** Expression of homologous recombination genes (https://www.genome.jp/entry/hsa03440) from targeted capture panel. *, ANOVA adj.p <0.05 versus Cluster 1. Points represent individual cells. **(E)** Haircut assay from hairpin DNA repair substrates that require activity of the indicated enzymes for editing and sequence readout. ****, ANOVA adj.p <0.0001, –E2 vs +E2. Points represent individual cells. **(F)** Repair of the Abasic hairpin yields two outcomes; APE1-mediated incision at an abasic site is followed by processing by either Polβ (short-patch repair, Abasic.1 - top) or Polδ/β and FEN1 (long-patch repair, Abasic.2 - bottom). *, ANOVA adj.p <0.05 versus Cluster 5. Points represent individual cells.

dysfunctional HR-mediated DNA repair in ILC cells. Based on this, we examined DNA repair foci by immunofluorescence, using RAD51 foci as a marker of HR initiation and resolution [37]. We found that ILC cells did form RAD51 foci in response to either ionizing radiation or etoposide, however, foci formation was notably delayed in ILC cells (MM134, 44PE) relative to IDC cells (T47D, HCC1428), particularly in response to ionizing radiation (**Figure 4C**). IDC cells formed RAD51 foci within 4 hours of radiation, with marked resolution of RAD51 foci by 24 hours, while ILC cells showed no substantial induction of RAD51 foci until 24 hours post-damage. Coupled with the lack of RAD51 protein turnover, these data suggest that complete execution and resolution of HR may be dysfunctional in ILC cells.

MDC1 plays a central role in the "decision" between HR and NHEJ, and MDC1:RAD51 association was shown to be critical for HR [36]. RAD51 was not detected in our IP/MS studies, so we examined this by co-IP with immunoblotting. We confirmed in MCF7 (IDC) that MDC1 was strongly associated with RAD51, and confirmed the decrease in RAD51 after etoposide treatment (**Figure 4D**). Conversely, we detected minimal MDC1:RAD51 association in MM134 (ILC) and saw no decrease in RAD51 via MDC1 co-IP after DNA damage. Collectively these data are consistent with inefficient or dysfunctional resolution of HR in ILC cells.

To further examine resolution of double-strand break repair via NHEJ versus HR, we utilized the 'Traffic Light' I-SceI fluorescent reporter system, which tracks repair pathway choice of NHEJ versus HR at an individual double-strand break in individual cells [38]. We integrated the Traffic Light reporter into ILC and IDC cells (see Materials and Methods), and tracked DNA repair choice per cell after induction of I-SceI by flow cytometry measurement for RFP (NHEJ) versus GFP (HR). Overall NHEJ activity was comparable across ILC and IDC cell lines, however, HR activity was extremely limited in ILC cells; HR accounted for ~6-10% of repair events in ILC cells, versus ~25% of events in IDC cells (**Figure 4E**; HCC1428 are functionally a *BRCA2*-hypomorph [39]). Taken together, these data support that HR is dysfunctional in ILC cells, and that this dysfunction may not prevent initiation of HR yet ultimately results in ineffective resolution of HR.

ILC tumors present features of a novel form of DNA repair dysfunction distinct from HR deficiency

Studies to date on HR deficiency related to "BRCAness" do not mechanistically account for the distinct form of dysfunctional, inefficient resolution of HR that presents in our data. As such, we revisited TCGA analyses, including the Pan-Cancer analysis of HR deficiency phenotypes [40] to identify features of ILC (focusing on ER+, Luminal A cancers) that may provide insight into this phenotype and its prevalence across ILC. In the TCGA analyses of Luminal A/ER+ ILC, high-risk ILC with the poorest survival had an elevated DNA Damage Response (DDR) score in reverse phase protein array (RPPA) analyses [4]. We examined whether increased DDR protein levels predicted outcomes similarly in ILC versus IDC in TCGA data; despite limited survival events among ILC in TCGA, high DDR protein levels predicted poorer overall survival in ILC, but not IDC (**Figure 5A**), supporting that the role of DDR proteins in disease etiology is distinct for ILC. Among these DDR proteins, RAD51 is substantially elevated in ER+ ILC vs IDC (**Figure 5B-C**), despite significantly lower *RAD51* mRNA levels in ER+ ILC (**Figure 5D**), suggesting RAD51 is increased post-transcriptionally e.g. via dysfunctional post-HR turnover. Further, while RAD51 protein and mRNA levels are positively correlated in ER+ IDC, no correlation is present in ER+ ILC (**Figure 5E**). These observations are consistent with our cell line data and support that resolution of DSB via HR is inefficient or dysfunctional in at least a subset of ILC.

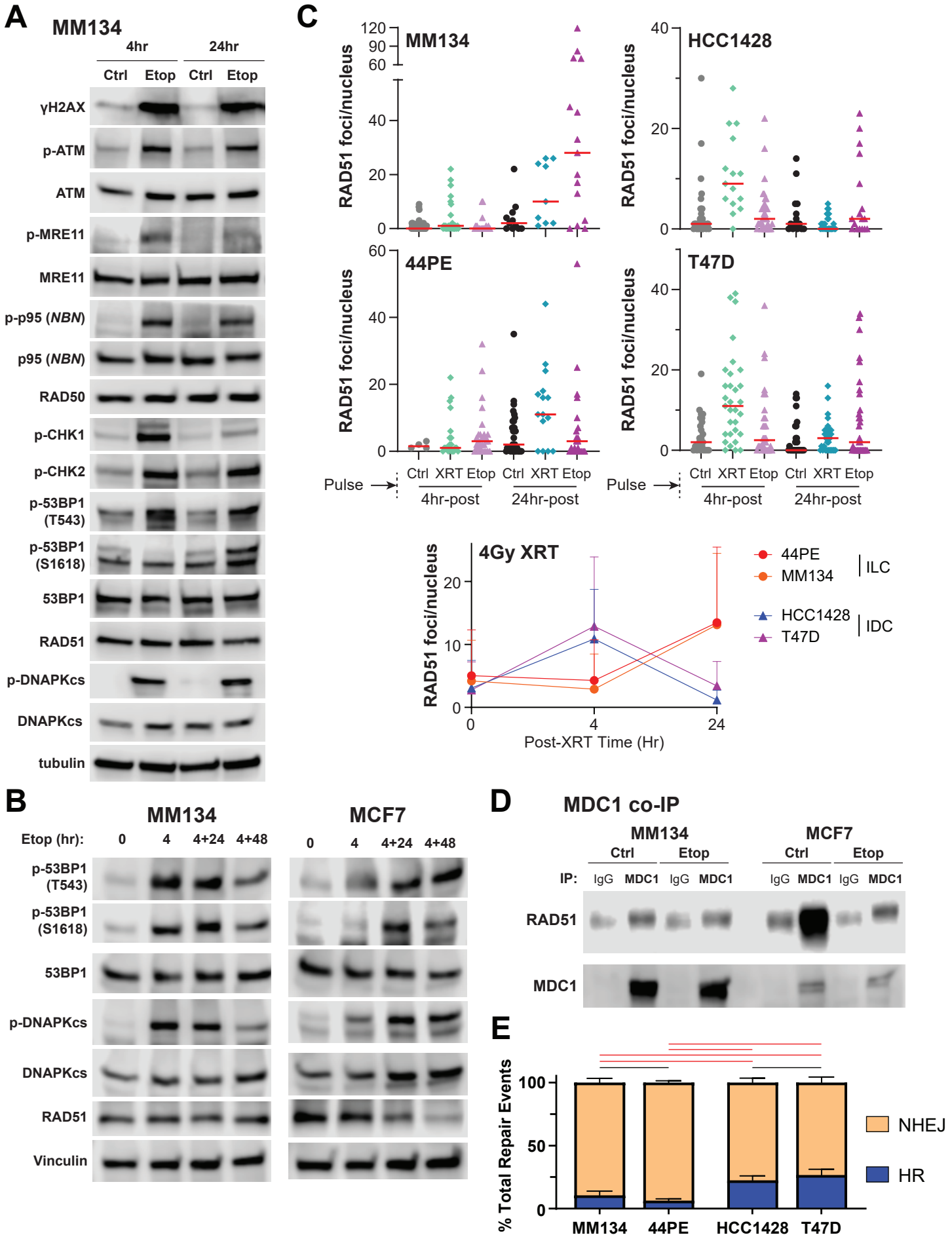

Figure 4. Activation of HR is limited and delayed in MM134 (ILC) versus MCF7 (IDC) cells. (A) MM134 cells treated with 10μM etoposide for 4 or 24 hours were analyzed by western blot for canonical interactors of MDC1 (γH2AX, ATM, and MRN) and down-stream mediators of canonical MDC1 signaling (CHK1/2, 53BP1, RAD51, and DNAPKcs). **(B)** Western blot comparison of MM134 (ILC) and MCF7 (IDC) for MDC1 interaction of downstream NHEJ (53BP1 and DNAPKcs) vs HR (Rad51) was performed. Increased turnover of RAD51 in MCF7 is suggestive of HR being used to repair etoposide induced double strand breaks. **(C)** Breast cancer cells were treated with a 4hr pulse of 10μM etoposide, or 4Gy ionizing radiation, and allowed to recover for 4 or 24hr prior to assessing RAD51 foci formation by immunofluorescence. Points represent foci counts in individual nuclei, read line represent median per condition. **(D)** Immunoprecipitation of MDC1 in MM134 and MCF7 cells treated with 10μM etoposide. Increased co-IP of RAD51 is observed in MCF7 but not MM134. **(E)** TrafficLight DNA repair reporter output from breast cancer cells. Bars represent mean ± SD form n=5 biological replicates. Red bar represents ANOVA $p<0.05$ for indicated comparison.

While the TCGA Pan-Cancer analyses of HR deficiency phenotypes provided a comprehensive analysis across tumor types, subgroup analyses for ILC was not reported yet shows striking differences in DNA damage response phenotypes in ILC. Despite the putative HR dysfunction identified in ILC, none of the genomic markers of HR deficiency were increased in ILC [40,41], and were essentially all decreased in ILC compared to IDC, including HR deficiency markers associated with telomeric allelic imbalance [42], large-scale transitions [43], and loss-of-heterozygosity events [44] (**Figure 5F**). Collectively, the absence of genomic scarring associated with overt HR deficiency in ILC tumors is consistent with our mechanistic data. Notably, the single elevated signature suggesting HR deficiency in ILC is PARPi7 score (**Figure 5G**). PARPi7 is a normalized gene expression score predictive of sensitivity to PARP inhibitors ([45]; high *CHEK2* and *MAPKAPK2*, with low *BRCA1*, *MRE11*, *NBN*, *TDG*, and *XPA* drive high PARPi7 score), which is validated in I-SPY clinical trials. High PARPi7 score predicted pathologic complete response in high-risk, ER+ breast cancer in response to PARPi veliparib + carboplatin [46] or PARPi olaparib + durvalumab [47]. Notably, the increased PARPi7 in ILC is likely functionally significant, as cutoffs of 0.0372 and 0.174 separated PARPi-sensitive versus -resistant tumors using Affymetrix and Agilent data, respectively [45,46]. Absent a trial-defined cutoff for RNAseq data, at a more conservative cutoff of 0.2, 49% of Luminal A ILC vs 28% of Luminal A IDC are PARPi7-high (X^2 test, p=0.000018); this cutoff identified poor disease-free survival in ILC, but not IDC (**Figure 5H**). With the disconnect between PARPi7 score and other markers of genomic scarring, this observation supports that HR dysfunction in ILC is distinct from current measures of overt HR deficiency.

ILC cells are sensitive to PARP inhibitor talazoparib in vitro and in vivo

With evidence that ILC cell lines and tumors present with HR dysfunction, links between MDC1 co-regulator function and reliance PARP-mediated DNA repair, and the elevated PARPi7 scores observed in ILC tumors, we examined whether ILC cells are sensitive to PARP inhibition. We focused on FDA-approved agent talazoparib, which more potently traps PARP1/2 on DNA relative to olaparib [49]. Via live cell Incucyte imaging we found that ILC cell lines MM134 and 44PE are sensitive to low-nanomolar concentrations of talazoparib (**Figure 6A**), similar to MCF-7 but ~10-fold more sensitive than T47D cells. Parallel experiments measuring cell proliferation by dsDNA quantification confirmed low-nanomolar talazoparib sensitivity in ILC cells (**Figure 6B**, **Supplemental Figure 4A**). Notably, both confluence and dsDNA quantification time-courses suggested that the impact of talazoparib treatment on ILC cells manifested at 5-6 days post-treatment, and that remaining ILC cells were likely less viable after talazoparib treatment versus IDC cells (**Supplemental Figure 4A-B**). To examine post-treatment cell viability, we washed out drug and re-plated cells after the 7 day treatment, and assessed outgrowth. ILC cell lines MM134 and 44PE, but not IDC lines MCF7 and T47D, remained significantly growth inhibited after drug washout (**Figure 6C**), suggesting that PARPi treatment had a long-term impact on cell viability specifically in ILC cells.

Our data suggests that PARPi sensitivity in ILC is linked to ER:MDC1 activity and HR capacity, which we were able to examine using our long-term estrogen deprived variants (LTED, modeling aromatase inhibitor resistance) of MM134 (134:LTED) and 44PE (44:LTED) [50,51]. We previously showed that though these models are ER+, 134:LTED are ER-independent while 44:LTED are ER-dependent. Accordingly, 134:LTED are not growth-inhibited by fulvestrant or MDC1 knockdown, while 44:LTED remain sensitive to both fulvestrant and MDC1 knockdown (**Figure 6D**), and the ER:MDC1 interaction is lost versus maintained in 134:LTED versus 44:LTED, respectively (**Figure 6E**). These observations suggest that MDC1 is maintained as

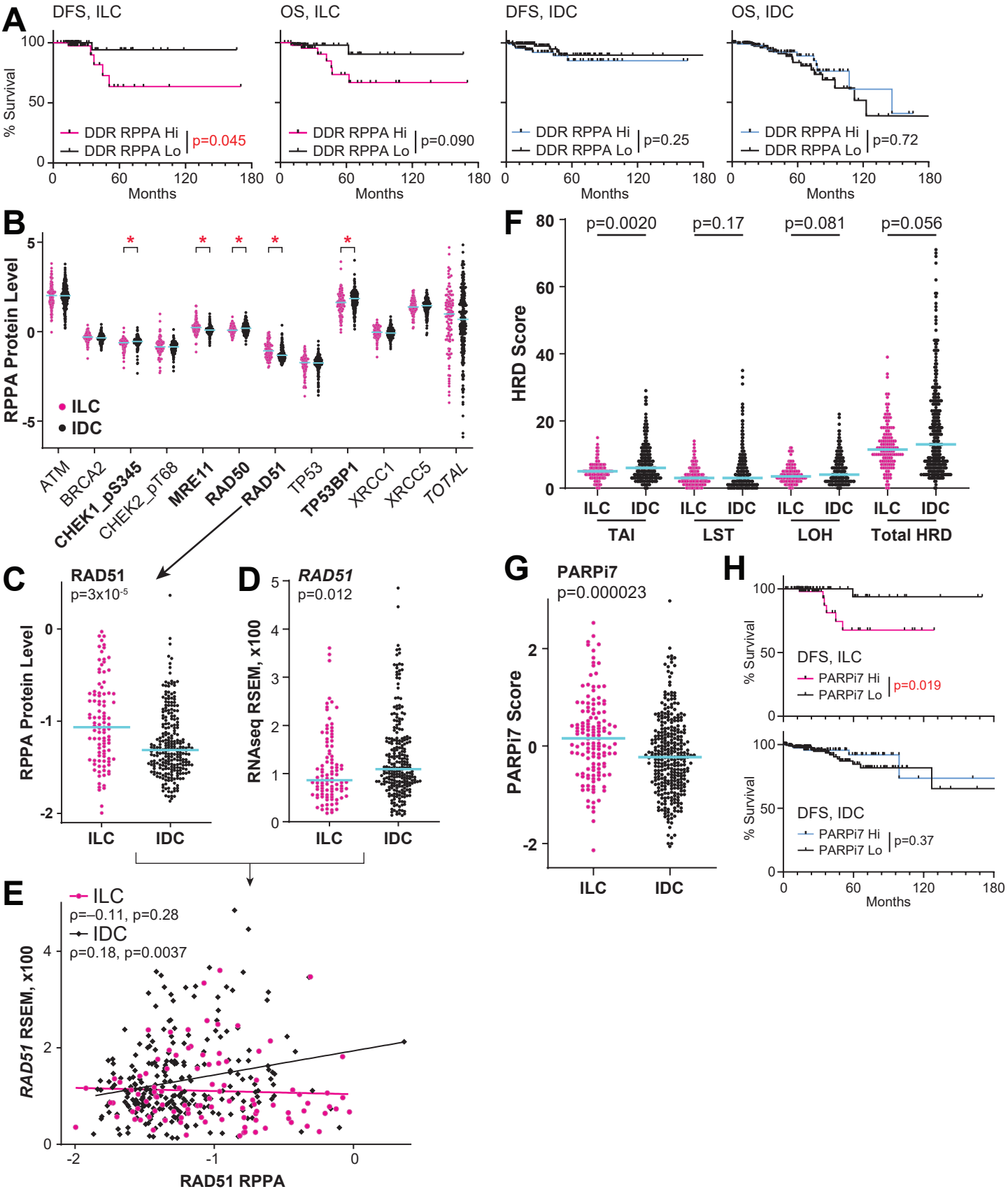

Figure 5. Protein array data are consistent with DNA repair dysfunction in ILC tumors and cell lines. mRNA, protein, and associated clinical data downloaded from cBio Portal [77], TCGA PanCan dataset; HRD feature data from [40]. **(A)** Disease-free survival (DFS) and Overall Survival (OS) for Luminal A tumors with available RPPA data. Hi/Lo defined by total RPPA signal sum cutoff of 1. ILC RPPA Hi: DFS n=42, OS n=49; ILC RPPA Lo: DFS n=46, OS n=50; IDC RPPA Hi: DFS n=98, OS n=111; IDC RPPA Lo: DFS n=112, OS n=139. Log-rank test p-value shown. IDC curves are ended at 180mo but no survival events occurred >180mo. **(B)** Normalized RPPA signal shown per target. ILC n=99, IDC n=251. Blue line = median. *, Mann-Whitney with FDR < 5% (adj.p < 0.05). **(C)** RAD51 RPPA data, as in (B). **(D)** *RAD51* mRNA expression. Mann-Whitney T-test p-value shown. **(E)** RPPA vs mRNA data from (C-D); Spearman correlation statistics shown.**(F-G)** Homologous recombination deficiency (HRD) scores shown, representative of other trends observed in Luminal A tumors in [40], and PARPi7 score from same dataset. ILC n=134; IDC n=315. Blue line = median. Mann-Whitney T-test p-value shown. **(H)** DFS from samples with PARPi7 score and survival data. ILC PARPi7 Hi, n=57; ILC PARPi7 Lo, n=62; IDC PARPi7 Hi, n=82; IDC PARPi7 Lo, n=188. Log-rank test p-value shown. IDC curves are ended at 180mo but no survival events occurred >180mo.

a transcriptional partner of ER in 44:LTED, but may be de-coupled from ER in 134:LTED and thus potentially can re-engage in DDR activity. Using the Traffic Light reporter, we found that while 44:LTED perform limited HR as seen in parental 44PE, HR activity is strongly increased in 134:LTED, consistent with a restoration of HR activity (**Figure 6F**). Ultimately this restoration of HR activity was accompanied by a decrease in sensitivity to talazoparib specifically in 134:LTED, which were >50-fold less sensitive to the PARPi versus parental MM134 cells (**Figure 6G**). Together these data support that differential activity of MDC1 in DDR underpins responsiveness to PARPi in ILC cells.

We next examined single-agent talazoparib efficacy *in vivo* using mammary fat pad xenograft tumors of MM134 cells in female immunocompromised mice (NSG, NOD.Cg-*Prkdc*^{scid} *Il2rg*^{tm1Wjl}/SzJ). Mice were supplemented with 30μM estradiol in drinking water beginning 7 days prior to tumor challenge to support tumor growth, and 20 mice were injected with 5x10^6 MM134 cells in Matrigel bilaterally at the #4 mammary fat pad. Treatments were initiated at day 27 post-tumor challenge with >25% of tumors >100mm^3. n=5 mice per arm received vehicle (vehicle gavage, see Methods), talazoparib (0.33mg/kg; 5d/w p.o.) for 3 weeks, talazoparib for 6 weeks, or fulvestrant (5mg/kg s.c. weekly) for 6 weeks; tumors were tracked until all vehicle control mice reached humane study endpoints (≥15mm tumor diameter, day 79). Of note, the 6-week talazoparib arm was lost at day 72 due to a cage flood and data are censored and excluded from analysis. In this study, single agent talazoparib (Tala) treatment significantly suppressed tumor growth versus control (ANOVA Vehicle vs 3wk Tala, p<0.0001), and outperformed fulvestrant in reducing tumor growth (ANOVA Fulvestrant vs 3wk Tala, p=0.0035) (**Supplemental Figure 5A**). Fulvestrant provided an initial growth suppression, but several tumors continued to grow on active treatment. Conversely, though talazoparib treated tumors were larger than at study initiation (3wk Tala: ~2.9-fold increase at endpoint, paired t-test p=0.002), growth inhibition was durable and tumors did not significantly increase in volume between treatment completion and study endpoint (day 48 vs day 79, paired t-test p=0.11).

We then tested the efficacy of talazoparib alone or in combination with endocrine therapy, via fulvestrant or estrogen withdrawal (to model aromatase inhibitors, AI) against MM134 and 44PE xenografts. In these studies, treatment was maintained for 6 weeks and then tumor outgrowth was tracked after cessation. Tala alone suppressed tumor growth vs control in MM134 (ANOVA p=0.0016) but not 44PE; adding fulvestrant to Tala showed no additive effect for either cell line (**Supplemental Figure 5B-C**). However, combined AI+Tala was highly effective in both models, with AI+Tala superior to either single treatment against tumor growth (**Figure 7A-D**), and causing a durable slowing of tumor outgrowth after treatment cessation (**Figure 7A-B**). Both cell line xenografts were growth inhibited by estrogen withdrawal (i.e. AI treatment model), however, AI+Tala caused a greater decrease in tumor volume at endpoint for both models (**Figure 7C-D**). Notably, AI alone caused a modest decrease in tumor volume in 44PE with 1/10 tumors increasing in size by treatment completion (25±37% decreased volume, paired ANOVA p=0.06), while AI+Tala was more effective (56±27% decreased volume, paired ANOVA p=0.0006). These data support that ILC cells are sensitive to PARPi despite the absence of classical HR-deficiency, and mechanistically implicate ER:MDC1 activity in HR dysfunction and thus PARPi sensitivity.

Based on our efficacy data, testing PARPi combinations *in vivo* against anti-estrogen-resistant ILC models is critical, however, our LTED cell lines have shown very limited engraftment as mammary fat pad xenografts (not shown) in contrast to the parental cell lines. To examine PARPi efficacy against anti-estrogen-

resistant ILC, we utilized the patient-derived xenograft (PDX) model HCI-013, which was derived after that patient had received letrozole (AI) + leuprolide, tamoxifen, and exemestane (AI), followed by several chemotherapy regimens; HCI-013 also carries the *ESR1*^{Y537S} mutation [52,53]. After 10 weeks treatment with Tala ± AI (estrogen withdrawal), AI+Tala caused the strongest suppression of PDX growth (**Figure 7E-F**). AI alone did limit tumor growth versus control (**Figure 7E**), but 30% of tumors (6/20) had increased in size during treatment (**Figure 7F**). No progression was observed with AI+Tala and 30% of tumors (6/20) were non-palpable at treatment completion, while AI+Tala-treated tumors were significantly smaller than AI alone at endpoint (**Figure 7F**) (AI: 27±42% decreased volume, versus AI+Tala: 76±20% decreased volume; post-treatment volume, AI: 106±55mm^3 versus AI+Tala: 46±55mm^3, ANOVA $p<0.0001$).

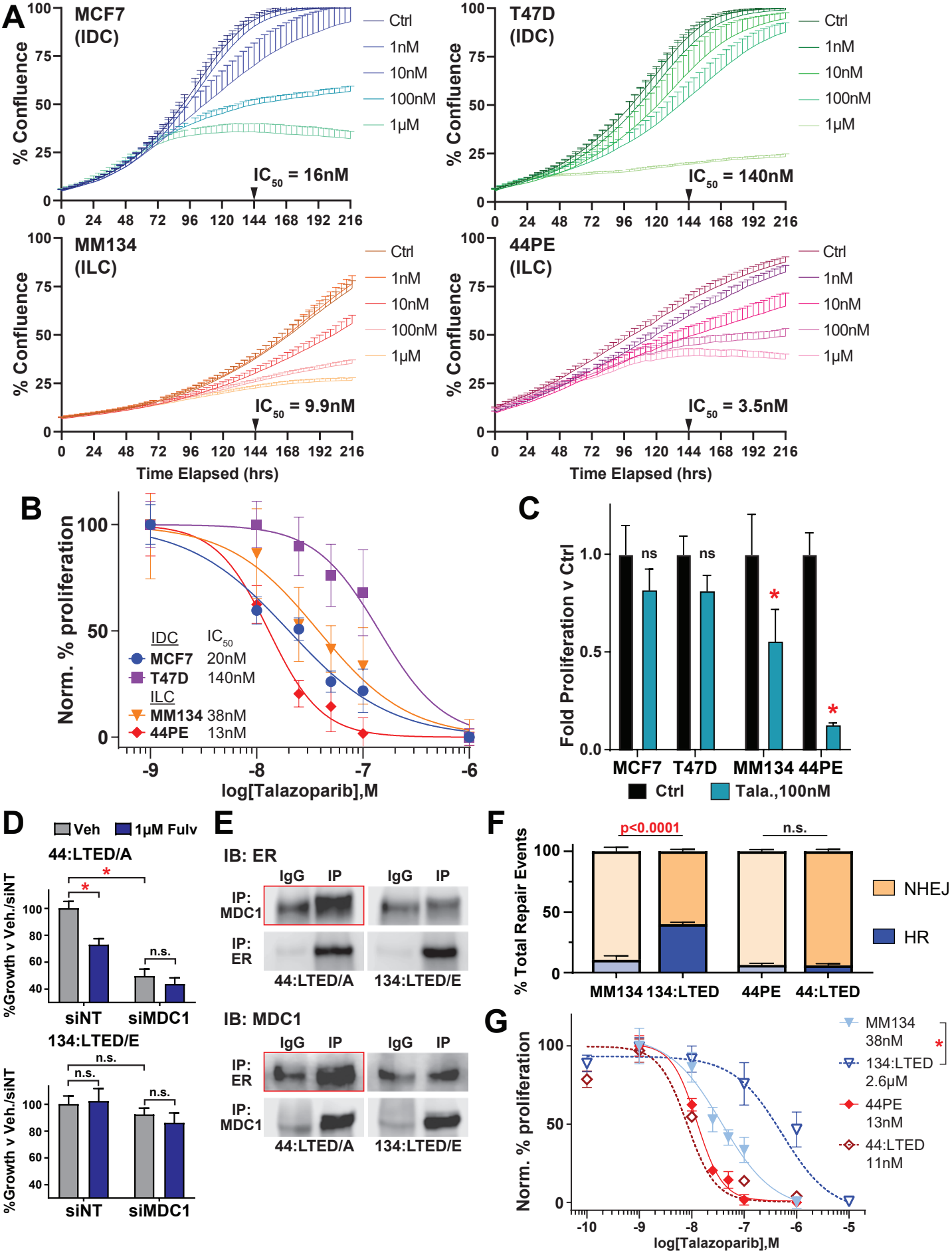

Figure 6. ILC cells *in vitro* are sensitive to PARP inhibitor talazoparib. (A) Representative growth curves via confluence in live cell imaging (Incucyte) for ILC vs IDC cells with increasing concentrations of talazoparib. IC_{50} calculated using percent confluence at 144hr post-treatment. Line represents mean confluence of 6 replicates ± SD. **(B)** Proliferation at 7d (168hr) as assessed by dsDNA quantification, shown as normalized % proliferation vs max/min. Points represent mean of 6 replicates ± SD. **(C)** Proliferation at 7d post drug washout (14d after initial treatment) by dsDNA quantification. Bars represent mean of 6 replicates ± SD. *, ANOVA, Ctrl v Tala $p<0.05$. **(D)** Proliferation at 7d as in (B-C) after siRNA transfection or indicated treatment. /A and /E designations indicate representative LTED sub-lines used in studies herein, from [50]. **(E)** Reciprocal co-immunoprecipitation of MDC1 versus ERα (ER). Red boxes highlight 'target' co-IPs confirming ER:MDC1 association in 44:LTED/A, which is not enriched versus IgG control in 134:LTED/E. **(F)** TrafficLight reporter as in Figure 4E, data for parental cells replicated from Figure 4E for clarity. ANOVA p-value shown. **(G)** Proliferation at 7d with increasing talazoparib concentration, as above. Dose-response curves for parental cells from Figure 6B shown for clarity. *, IC_{50} comparison $p<0.05$.

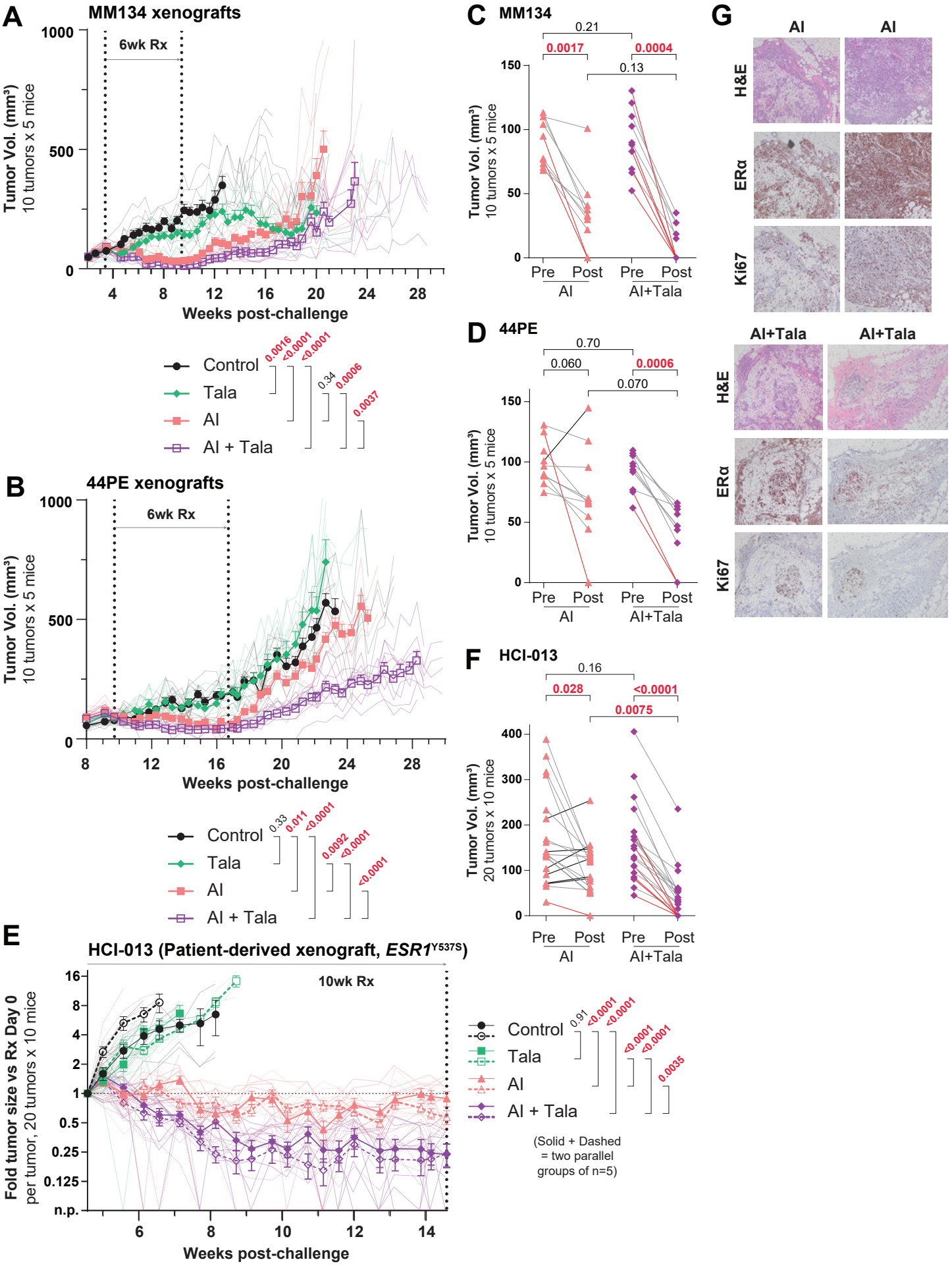

Figure 7. Talazoparib causes sustained growth suppression in MM134 xenograft tumors. (A-B) Bold lines/symbols show mean tumor size ± SEM; individual tumor size shown as matching faded lines. Bold lines ended at first tumor size human endpoint reached per arm. Two-way ANOVA treatment effect p-values shown. **(C-D**) Tumor volume at treatment initiation vs completion for studies in (A-B). Red lines = tumor non-palpable at treatment completion; Black lines = increased tumor volume at treatment completion vs initiation. Paired ANOVA p-values shown. **(E)** Tumor growth shown as fold-change in tumor size versus treatment initiation. Bold/faded lines as above; two-way ANOVA includes all 20 tumors per treatment arm together. n.p. = non-palpable at measurement timepoint (volume = 0 for ANOVA). **(F)** Change in tumor volume for HCI-013 as in (C-D). **(G)** Representative immunohistochemistry from tumors collected at 10-week treatment completion for AI and AI+Tala tumors.

DISCUSSION

Patients diagnosed with ILC are faced with distinct treatment and clinical management challenges, in part related to uniquely poor long-term outcomes, controversy around the efficacy of anti-estrogens, and a lack of biomarker and therapy strategies based on ILC biology. Toward better understanding estrogen and anti-estrogen response in ILC, we previously identified that the DNA repair protein MDC1 has novel ER co-regulator activity in ILC cells that mediates estrogen response and anti-estrogen resistance, yet is associated with putative DNA repair dysfunction [14]. In the present study, we profiled the MDC1 interactome to characterize MDC1 function in DNA repair, versus MDC1 as a transcriptional regulator, in IDC versus ILC cells. MDC1 associations with homologous recombination proteins were depleted in ILC cells, mirroring that observed in *BRCA2*-mutant IDC cells. Using single-cell transcriptomics paired with DNA repair activity measured with the 'Haircut' assay, we found that ER:MDC1 gene regulation activity was associated with an upregulation of PARP-mediated repair pathways, specifically increased activity of base excision repair. Functional studies of DDR initiation, propagation, and resolution suggested that ILC cells ultimately show support that ILC cells have a distinct form of DNA repair dysfunction, and we tested whether this dysfunction could be exploited using FDA-approved PARPi talazoparib. Both *in vitro* and *in vivo*, ILC cells were sensitive to talazoparib, which caused durable suppression of cell/tumor growth after treatment cessation. Understanding how MDC1 underpins ILC-specific ER functions and DNA repair dysfunction offers a path toward ILC precision therapies based on identifying tumors where MDC1 activity indicates PARPi sensitivity.

ILC are not associated with typical features of DNA repair deficiency or sensitivity to DNA damage – in addition to the limited genomic scars of overt HR deficiency we noted in TCGA data, and depletion of associated germline mutations in ILC [20–22], ILC generally have limited response to chemotherapy [2,54]. However, our data taken together with observations in the literature suggest that ILC may present with DNA repair dysfunction that does not manifest as HR deficiency (HRD) as currently understood. HR dysfunction in ILC may be linked to the elevated DNA damage response signature and DDR protein levels in ILC (in TCGA), which supports that DDR plays a distinct role in ILC etiology, particularly aggressive ILC associated with poor outcomes. The mechanistic significance of the elevated DDR signature is unknown, but the lack of RAD51 turnover we observed suggests that elevated DDR protein levels could be due to inefficient or dysfunctional resolution of DDR. Given that current HRD signatures are largely trained using primarily *BRCA1/2*-mutant tumors, more subtle dysfunction may not be captured. In that context, mutations in other HR genes are often only linked to high HRD scores in a tissue type-dependent manner [55], which thus may include ILC. Similarly, we observed that ILC cells were competent to form RAD51 foci upon damage (which would otherwise suggest ILC cells are HR-proficient [37]) despite showing little HR-mediated repair in I-SceI reporter assays. Identifying the mechanistic underpinning of HR dysfunction is an important future direction. Notably, the restoration of the HR-associated MDC1 interactome upon fulvestrant treatment, and the restoration of HR activity in 134:LTED cells, suggests that the HR dysfunction is dynamic or otherwise transient, via active regulation of MDC1 or associated factors (e.g. ER or related epigenomic factors). Indeed, increased HR activity in 134:LTED was associated with talazoparib resistance in those cells, highlighting that understanding HR dysfunction and regulation is critical toward understanding PARPi sensitivity in ILC.

Defining the connection between DDR dysfunction and tumor mutational burden (TMB) in ILC may also yield important insight into DNA repair capacity and PARPi sensitivity in ILC. Other studies have reported

in multiple cohorts that ILC present with a substantial enrichment in APOBEC-driven mutational signatures compared to matched IDC tumors. APOBEC signatures are enriched in ~16-38% of primary ILC (vs 8-16% of primary IDC/NST) and 22-51% of metastatic ILC (vs ~10-28% of metastatic IDC/NST) [56–58], and are associated with increased TMB relative to APOBEC-negative tumors, mirroring the increased overall TMB reported in metastatic ILC [24]. Given that APOBEC lesions are repaired by PARP-driven pathways, high APOBEC activity has been associated with PARPi-sensitivity [59,60]; high APOBEC activity combined with HR dysfunction may impart PARPi sensitivity in ILC without otherwise driving broad HRD-related scarring.

Though PARP inhibitors including talazoparib have been extensively tested in breast cancer, their clinical efficacy for ILC, especially beyond *BRCA1/2*-mutant tumors, is unknown. The phase III olaparib trial OlympiAD did not report tumor histology in initial results or subgroup analyses, and the two largest breast cancer trials of talazoparib reported to date (EMBRACA [61] and ABRAZO [62]) did not report tumor histology. A pilot neoadjuvant talazoparib study [63] included one germline *BRCA2*-mutant patient with ER+ ILC which had a pathologic complete response to talazoparib, but the extended version of the trial, NEOTALA, did not report tumor histology [64]. Defining biomarkers for DNA repair activity and/or MDC1 repair vs genomic activity in ILC is critical to better understand the scope of DNA repair dysfunction in ILC and to design effective trials for talazoparib in ILC.

It is important to consider that though *TP53* mutations are uncommon in ILC, the cell line models used in our studies (with the exception of MCF7) do carry *TP53* mutations, which is typical of cancer cell lines including ILC [65–67]. However, MM134 and 44PE do mirror 'Proliferative' ILC regarding the elevated DNA damage response protein signature [68], yet few other models of ER+/HER2-negative ILC exist. Recent multi-omic profiling of putative ILC models supports that among 5 luminal-type ILC cell lines, MM134 and 44PE are suitable models of ER+/luminal ILC, while BCK4 and MDA MB 330 are HER2-positive (via mutation and amplification, respectively), and CAMA1 has little transcriptional similarity to ILC tumors [67]. PDX of ER+ ILC are similarly limited; though some biobank reports have noted inclusion of ILC, HCI-013 is the only ER+ classic ILC PDX (i.e. not mixed ILC/NST) used in both drug treatment and endocrine-response studies in the literature to date [52,65]. Functional studies of DDR/HR and PARPi response in additional models - as ILC become increasingly represented - will be important to dissect DDR capacity and HR-related biomarkers.

It is becoming increasingly urgent to develop treatment strategies centered on a differential diagnosis of breast cancer of no special type (i.e. IDC), versus a diagnosis of ILC. In contrast to the lack of histology information in most trials, a recent series of clinical studies have enriched for or are specifically enrolling patients with ILC (e.g. ROSALINE [69], GELATO [70], NCT02206984). New prognostic signatures developed based on ILC tumors have been reported [71], and pre-clinical studies focusing on ILC models are beginning to identify and define ILC-specific biology toward ILC-tailored treatments [14,51,72–74]. Our data advance this paradigm of targeting ILC biology, and show that ILC-specific association between ER and MDC1 creates a new context for ER and MDC1 function in ILC, yet creates a putative synthetic vulnerability, i.e. a DNA repair dysfunction that may be exploitable with PARPi.

MATERIALS AND METHODS

Cell culture

MDA MB 134VI (MM134; ATCC HTB-23) and SUM44PE (44PE; Asterand/BioIVT) were maintained as described [52]. HCC1428 (ATCC CRL-2327), MCF7 (Rae Lab, U. Michigan) and T47D (Sartorius Lab, U. Colorado) were maintained as described [14]. 134:LTED (subline 134:LTED/E) and 44:LTED (subline 44:LTED/A) were maintained in estrogen-depleted conditions as described [50]. 293FT cells (Invitrogen) were maintained according to manufacturer directions. Cells were incubated at 37°C in 5% CO_2. All lines were regularly confirmed mycoplasma negative (MycoAlert, Lonza), and authenticated by STR profiling at the U. Colorado Anschutz Tissue Culture Core. Estradiol (E2) was from Sigma; ICI 182780 (fulvestrant; fulv) was from Tocris Biosciences. Etoposide and talazoparib (BMN-673) were from Cayman Chemical Company. Small molecules were dissolved in ethanol or DMSO, and vehicle treatments use 0.01-0.1% EtOH or DMSO *in vitro*.

MDC1 co-immunoprecipitation and mass spectrometry

Immuno-precipitation (IP) was performed as previously described [14]. Briefly, nuclear extract (NE) was prepared from successive hypotonic/hypertonic washes and lysing, then utilized for immunoprecipitation. 10µg antibody was used with NE for immunoprecipitation. Jackson ImmunoResearch Chromapure Mouse IgG was used for control. α-MDC1 (Sigma M2444) was used for MDC1 IP. NE was incubated with antibody overnight at 4°C with rotation, then extracted with magnetic A/G beads for 4hr at 4°C with rotation. For IP/mass spectrometry, bead-complexes were submitted intact to the Mass Spectrometry Core Facility at the University of Colorado – Boulder for sample preparation and analysis, using an Orbitrap nanoLC-MS. For IP followed by immunoblot, protein complexes were eluted by re-suspending beads in Laemmli-based buffer.

MDC1-IP/MS iBAQ values were used for comparison. IgG iBAQ values were subtracted as background from MDC1-IP values for all proteins. Only proteins enriched (i.e. background subtracted iBAQ > 0) were included in subsequent analyses. Genes present in GO genesets GO:0006397, GO:0000398, GO:0000377, GO:0006364, and GO:0042254 (related to RNA metabolism, see Supplemental File 1) were excluded from analysis as indicated in the text. MDC1 co-immunoprecipitated genes in 293FT (n=1666) were compared to Salifou et al [27] for validation of our IP/MS method. Enriched gene lists for each cell line were analyzed using EnrichR [75] for gene set enrichment analysis. Hierarchical clustering of gene sets was performed using Morpheus (https://software.broadinstitute.org/morpheus).

Single cell transcriptomics and Haircut analyses

MM134 cells were hormone-deprived in medium supplemented with charcoal-stripped FBS as previously described [76], then treated with vehicle (0.01% ethanol) or 100pM estradiol for 24hrs. After treatment, single cell suspensions were prepared according to 10X Genomics recommendations, and as described [32,33]. Whole transcriptome and Haircut libraries were prepared as described [32,33], and separate targeted capture libraries were prepared according to the manufacturer's instructions (https://www.10xgenomics.com/products/targeted-gene-expression). Supplemental File 2 includes workflow information and normalized gene expression data for the targeted capture panel and Haircut probes, with single-

cell annotation for clustering, cell cycle prediction, and ER target genes scores, and is available at: https://osf.io/rw2n6. Raw data will be made available upon submission for publication, or upon request.

Immunoblotting

Cells were seeded in 12-well plates for ~80% confluence (MM134: 800k/well; MCF7: 320k/well) and treated as indicated prior to lysis with RIPA buffer (Thermo Pierce). Primary antibodies were diluted to manufacturer recommended concentrations, in TBS + 0.05% Tween-20. Membranes were imaged on LiCor C-DiGit blot scanner. Primary antibodies for immunoblots were: phospho-Histone H2A.X (Ser139)(20E3) (Cell Signaling Technology #9718); ATM (D2E2) (Cell Signaling Technology #2873); Phospho-ATM (Ser1981)(D6H9)(Cell Signaling Technology #5883); MRE11 (31H4)(Cell Signaling Technology #4847); phosph-MRE11 (Ser676)(Cell Signaling Technology #4859); p95/NBS1 (NBN) (D6J5I)(Cell Signaling Technology #14956); phospho-p95/NBS1 (NBN)(Ser343)(Cell Signaling Technology #3001); Rad50 (Cell Signaling Technology #3427); phospho-CHK1 (Ser345)(133D3)(Cell Signaling Technology #2348); phospho-CHK2 (Thr68)(C13C1)(Cell Signaling Technology #2197); 53BP1 (E7N5D) XP (Cell Signaling Technology #88439); phospho-53BP1 (Ser1618)(D4H11)(Cell Signaling Technology #6209); phospho-53BP1 (Thr543)(Cell Signaling Technology #3428); Rad51 (D4B10)(Cell Signaling Technology #8875); DNA-PKcs (3H6)(Cell Signaling Technology #12311); phospho-DNA-PKcs (Ser2056)(E9J4G)(Cell Signaling Technology #68716); α/β-Tubulin (Cell Signaling Technology #2148); Vinculin (E1E9V) XP (Cell Signaling Technology #13901); MDC1 (MDC1-50)(Sigma-Aldrich M2444).

DNA damage response and HRD scores

DNA repair protein levels, and associated clinical and tumor data, from the TCGA PanCancer dataset were downloaded from cBio portal [77]; data were most recently downloaded for verification in October 2024. Scores for genomic markers of HRD including PARPi7 score and associated scarring phenotypes [40] were downloaded from the Genomic Data Commons (https://gdc.cancer.gov/about-data/publications/PanCan-DDR-2018) and a combined clinical/genomic TCGA dataset from the Gerke Lab (https://github.com/GerkeLab/TCGAhrd).

Immunofluorescence

Cells were plated [MCF7 ($2x10^4$ cells per well), 44PE ($1x10^4$ cells per well), and MM134/44PE ($1x10^5$ cells per well)] in 8-well chamber slides (Nunc Tek Chamber Slide System; Thermo Scientific). 24 hours after plating, cells were treated with 0.01% DMSO, 10μM etoposide, or 4Gy of XRT (Multirad350 irradiator). At time points noted, media was aspirated, and cells fixed with 4% methanol free paraformaldehyde (PFA; Electron Microscopy services) for 10 minutes at room temperature. Slides were permeabilized with 0.2% Triton X-100 in PBS. Anti-RAD51 antibody (Abcam, ab176458) was diluted 1:500 in 3% BSA and incubated for 2 hours at room temperature (RT). Goat anti-rabbit Alexa-Fluor 488 conjugated secondary antibody (ThermoScientific; A32731) was diluted 1:1000 in 3% BSA, and incubated on slides for 1 hour at RT. Slides were mounted with SlowFade™ Diamond Antifade with DAPI (ThermoFisher Scientific) for flurescence imaging. CellProfiler software [78] was used for foci analysis. A DAPI mask was used to isolate nuclei as regions of interest for defining RAD51 foci.

Traffic Light Reporter Assay

The Traffic Light Assay [38] was performed as previously described, however, the TrafficLight reporter was stably integrated into MM134, 44PE, HCC1428, T47D, 134:LTED, and 44:LTED cells. I-SceI was transiently expressed to induce the double-strand break in the reporter via transient lentiviral transduction using an integrase-dead lentivirus (see below). 72 hours after transduction and I-SceI expression, cells were trypsinized, washed, and diluted in FACS buffer (PBS + 1mM EDTA + 25mM HEPES + 1% BSA) for flow cytometry. Repair events were counted via red vs green fluorescence compared to cells without transient I-SceI expression, on a Beckman Coulter Gallios561 cytometer (Indianapolis, IN, USA) at the U. Colorado Cancer Center Flow Cytometry Shared Resource. Data ere analyzed using Kaluza Analysis Software v2.1 (Beckman Coulter). Traffic Light Reporter (pCVL Traffic Light Reporter 2.1, Addgene #31483) and companion I-SceI vector (Addgene #31476) were a gift from Andrew Scharenberg. For Traffic Light reporter transduction, lentivirus was constructed in 293FT cells via co-transfection with psPAX2 (Addgene #12260, a gift from Didier Trono) and pMD2.G (Addgene #12259, a gift from Didier Trono). For transient I-SceI vector transduction, psPAX2 was replaced with psPAX2-D64V (Addgene #63586, a gift from David Rawlings & Andrew Scharenberg).

Cell proliferation and viability

Total double-stranded DNA was quantified by Hoechst 33258 fluorescence as described [79], as a surrogate for cell number. Live cell analysis was performed using an S3 Incucyte (Sartorius, Bohemia, NY, USA) with the U. Colorado Cancer Center Cell Technologies Shared Resource. MCF7 ($2x10^3$ cells per well), T47D ($3x10^3$ cells per well), MM134 ($2x10^4$ cells per well), and 44PE ($1.5x10^4$ cells per well) were plated in a 96-well format. 24 hours after plating, cells were treated with the noted concentrations of talazoparib and placed in the S3 Incucyte for 216 hours. For analysis, a confluence phase mask was used to determine relatively confluency. Alternatively, cells were pre-treated with talazoparib for 7 days prior to re-plating in the 96-well format, and subsequent analysis.

Animals and xenograft treatment studies

All animal studies were performed in in AALAC-approved facility with approval of the University of Colorado – Anschutz Medical Center Institutional Animal Care and Use Committee (IACUC). 6-8 week female NSG (NOD.Cg-*Prkdc*^{scid} *Il2rg*^{tm1Wjl}/SzJ; Jackson Laboratory strain 005557) mice were used for all experiments. Five mice per group were used for all *in vivo* experiments.

One week prior to tumor challenge, mice were initiated on 30μM 17β-estradiol (E2) supplemented in the drinking water. Mice were allowed to drink and eat ad libitum for the duration of the study. Mice were weighed weekly as weight loss >10% was used as an indicator of acute toxicity. For tumor challenge, tumor cells were diluted in a 50/50 mixture of HBSS and phenol red-free LDEV-free Matrigel (Corning; Corning NY, USA). Mice were anesthetized with isoflurane, abdomen shaved, and challenged with $5x10^6$ MM134 or 44PE cells in the bilateral #4 mammary fat pads. Treatment was initiated when >25% of tumors exceeded ~$100mm^3$, with fulvestrant (5 mg/kg, diluted in 10% ethanol and 90% peanut oil, administered subcutaneously weekly), talazoparib (0.33 mg/kg, diluted in water with 4% DMSO + 30% PEG300 (Sigma-Aldrich), administered by oral gavage daily excluding weekends), or estrogen withdrawal (E2 supplement removed from drinking water; E2 supplementation was restored at the end of the indicated treatment window). Tumors were measured twice weekly using calipers, and mice were weighed weekly; tumor volume (V) was calculated using the formula $V =$

(S^2 x L) / 2, where L = Longest tumor diameter, and S = shortest tumor diameter. Mice were euthanized when any tumor diameter reached 15mm as defined humane endpoints.

Viable cryopreserved fragments of PDX HCI-013 were obtained from the Preclinical Research Resource at the University of Utah Huntsman Cancer Institute. PDX tumors were maintained in NSG mice with 30μM E2 supplemented in the drinking water. As above, naïve recipient NSG mice were maintained on E2 water for 1 week prior to PDX transplantation. For transplant, tumor was excised from donor mice, chopped into ~1mm^3 fragments, and held in HBSS to await transplant. Recipient mice were anesthetized with isoflurane, abdomen shaved, then a small incision was made near the #4 nipple for a single fragment of PDX tissue implanted into the exposed fat pat, with the wound closed with surgical staples. Buprenorphine-SR/ER (Wedgewood Pharmacy; Swedesboro, NJ 08085) was administered for analgesia. PDX were implanted bilaterally. Mice were treated as described above.

Software

Statistical analyses and associated graphs were prepared with Graphpad Prism v10 (GraphPad Software, Boston, MA, USA).

REFERENCES

1. Sikora MJ, Jankowitz RC, Dabbs DJ, Oesterreich S. Invasive lobular carcinoma of the breast: patient response to systemic endocrine therapy and hormone response in model systems. Steroids. 2013 Jun;78(6):568–575. PMID: 23178159
2. Mouabbi JA, Hassan A, Lim B, Hortobagyi GN, Tripathy D, Layman RM. Invasive lobular carcinoma: an understudied emergent subtype of breast cancer. Breast Cancer Res Treat. 2022 Jun;193(2):253–264. PMID: 35347549
3. McCart Reed AE, Kalinowski L, Simpson PT, Lakhani SR. Invasive lobular carcinoma of the breast: the increasing importance of this special subtype. Breast Cancer Res BCR. 2021 Jan 7;23(1):6. PMCID: PMC7792208
4. Ciriello G, Gatza ML, Beck AH, Wilkerson MD, Rhie SK, Pastore A, et al. Comprehensive Molecular Portraits of Invasive Lobular Breast Cancer. Cell. 2015 Oct 8;163(2):506–519. PMCID: PMC4603750
5. Arpino G, Bardou VJ, Clark GM, Elledge RM. Infiltrating lobular carcinoma of the breast: tumor characteristics and clinical outcome. Breast Cancer Res BCR. 2004;6(3):R149-156. PMCID: PMC400666
6. Rakha EA, El-Sayed ME, Powe DG, Green AR, Habashy H, Grainge MJ, et al. Invasive lobular carcinoma of the breast: response to hormonal therapy and outcomes. Eur J Cancer Oxf Engl 1990. 2008 Jan;44(1):73–83. PMID: 18035533
7. Chen Z, Yang J, Li S, Lv M, Shen Y, Wang B, et al. Invasive lobular carcinoma of the breast: A special histological type compared with invasive ductal carcinoma. PloS One. 2017;12(9):e0182397. PMCID: PMC5580913
8. Foldi J, Carleton N, Anderson SJ, Rastogi P, Lee A, Balic M, et al. Long-term outcomes by lobular versus ductal histology in four NSABP adjuvant breast cancer trials. J Natl Cancer Inst. 2024 Aug 10;djae188. PMID: 39128018
9. Mathew A, Rajagopal PS, Villgran V, Sandhu GS, Jankowitz RC, Jacob M, et al. Distinct Pattern of Metastases in Patients with Invasive Lobular Carcinoma of the Breast. Geburtshilfe Frauenheilkd. 2017 Jun;77(6):660–666. PMCID: PMC5489406
10. Fitzpatrick A, Iravani M, Mills A, Vicente D, Alaguthurai T, Roxanis I, et al. Genomic profiling and pre-clinical modelling of breast cancer leptomeningeal metastasis reveals acquisition of a lobular-like phenotype. Nat Commun. 2023 Nov 16;14(1):7408. PMCID: PMC10654396
11. Metzger Filho O, Giobbie-Hurder A, Mallon E, Gusterson B, Viale G, Winer EP, et al. Relative Effectiveness of Letrozole Compared With Tamoxifen for Patients With Lobular Carcinoma in the BIG 1-98 Trial. J Clin Oncol. 2015 Sep 1;33(25):2772–2779. PMCID: PMC4550691
12. Riba LA, Russell T, Alapati A, Davis RB, James TA. Characterizing Response to Neoadjuvant Chemotherapy in Invasive Lobular Breast Carcinoma. J Surg Res. 2019 Jan;233:436–443. PMID: 30502283
13. Truin W, Voogd AC, Vreugdenhil G, van der Heiden-van der Loo M, Siesling S, Roumen RM. Effect of adjuvant chemotherapy in postmenopausal patients with invasive ductal versus lobular breast cancer. Ann Oncol. 2012 Nov;23(11):2859–2865. PMID: 22745216
14. Sottnik JL, Bordeaux EK, Mehrotra S, Ferrara SE, Goodspeed AE, Costello JC, et al. Mediator of DNA Damage Checkpoint 1 (MDC1) Is a Novel Estrogen Receptor Coregulator in Invasive Lobular Carcinoma of the Breast. Mol Cancer Res MCR. 2021 Aug;19(8):1270–1282. PMCID: PMC8349796
15. Jungmichel S, Stucki M. MDC1: The art of keeping things in focus. Chromosoma. 2010 Aug;119(4):337–349. PMID: 20224865
16. Coster G, Goldberg M. The cellular response to DNA damage: a focus on MDC1 and its interacting proteins. Nucl Austin Tex. 2010;1(2):166–178. PMCID: PMC3030693
17. Ruff SE, Logan SK, Garabedian MJ, Huang TT. Roles for MDC1 in cancer development and treatment. DNA Repair. 2020 Nov;95:102948. PMCID: PMC7669677
18. Lou Z, Minter-Dykhouse K, Franco S, Gostissa M, Rivera MA, Celeste A, et al. MDC1 maintains genomic stability by participating in the amplification of ATM-dependent DNA damage signals. Mol Cell. 2006 Jan 20;21(2):187–200. PMID: 16427009

19. Meyer B, Voss KO, Tobias F, Jakob B, Durante M, Taucher-Scholz G. Clustered DNA damage induces pan-nuclear H2AX phosphorylation mediated by ATM and DNA-PK. Nucleic Acids Res. 2013 Jul;41(12):6109–6118. PMCID: PMC3695524
20. Dossus L, Benusiglio PR. Lobular breast cancer: incidence and genetic and non-genetic risk factors. Breast Cancer Res BCR. 2015 Mar 13;17:37. PMCID: PMC4357148
21. Ditchi Y, Broudin C, El Dakdouki Y, Muller M, Lavaud P, Caron O, et al. Low risk of invasive lobular carcinoma of the breast in carriers of BRCA1 (hereditary breast and ovarian cancer) and TP53 (Li-Fraumeni syndrome) germline mutations. Breast J. 2019 Jan;25(1):16–19. PMID: 30414230
22. Yadav S, Hu C, Nathanson KL, Weitzel JN, Goldgar DE, Kraft P, et al. Germline Pathogenic Variants in Cancer Predisposition Genes Among Women With Invasive Lobular Carcinoma of the Breast. J Clin Oncol. 2021 Dec 10;39(35):3918–3926. PMCID: PMC8660003
23. Cao L, Basudan A, Sikora MJ, Bahreini A, Tasdemir N, Levine KM, et al. Frequent amplifications of ESR1, ERBB2 and MDM4 in primary invasive lobular breast carcinoma. Cancer Lett. 2019 Oct 1;461:21–30. PMCID: PMC6682463
24. Sokol ES, Feng YX, Jin DX, Basudan A, Lee AV, Atkinson JM, et al. Loss of function of NF1 is a mechanism of acquired resistance to endocrine therapy in lobular breast cancer. Ann Oncol. 2019 Jan 1;30(1):115–123. PMCID: PMC6336006
25. Gupta R, Somyajit K, Narita T, Maskey E, Stanlie A, Kremer M, et al. DNA Repair Network Analysis Reveals Shieldin as a Key Regulator of NHEJ and PARP Inhibitor Sensitivity. Cell. 2018 May 3;173(4):972-988.e23. PMCID: PMC8108093
26. Su D, Ma S, Shan L, Wang Y, Wang Y, Cao C, et al. Ubiquitin-specific protease 7 sustains DNA damage response and promotes cervical carcinogenesis. J Clin Invest. 2018 Oct 1;128(10):4280–4296. PMCID: PMC6159995
27. Salifou K, Burnard C, Basavarajaiah P, Grasso G, Helsmoortel M, Mac V, et al. Chromatin-associated MRN complex protects highly transcribing genes from genomic instability. Sci Adv. 2021 May;7(21):eabb2947. PMCID: PMC8139584
28. Heyza JR, Mikhova M, Bahl A, Broadbent DG, Schmidt JC. Systematic analysis of the molecular and biophysical properties of key DNA damage response factors. eLife. 2023 Jun 21;12:e87086. PMCID: PMC10319438
29. Sigismondo G, Arseni L, Palacio-Escat N, Hofmann TG, Seiffert M, Krijgsveld J. Multi-layered chromatin proteomics identifies cell vulnerabilities in DNA repair. Nucleic Acids Res. 2023 Jan 25;51(2):687–711. PMCID: PMC9881138
30. Ichijima Y, Ichijima M, Lou Z, Nussenzweig A, Camerini-Otero RD, Chen J, et al. MDC1 directs chromosome-wide silencing of the sex chromosomes in male germ cells. Genes Dev. 2011 May 1;25(9):959–971. PMCID: PMC3084029
31. Pappas G, Munk SHN, Watanabe K, Thomas Q, Gál Z, Gram HH, et al. MDC1 maintains active elongation complexes of RNA polymerase II. Cell Rep. 2023 Jan 31;42(1):111979. PMID: 36640322
32. Richer AL, Riemondy KA, Hardie L, Hesselberth JR. Simultaneous measurement of biochemical phenotypes and gene expression in single cells. bioRxiv. 2019 Oct 29;820233.
33. Richer AL, Riemondy KA, Hardie L, Hesselberth JR. Simultaneous measurement of biochemical phenotypes and gene expression in single cells. Nucleic Acids Res. 2020 Jun 4;48(10):e59. PMCID: PMC7261187
34. Inano S, Sato K, Katsuki Y, Kobayashi W, Tanaka H, Nakajima K, et al. RFWD3-Mediated Ubiquitination Promotes Timely Removal of Both RPA and RAD51 from DNA Damage Sites to Facilitate Homologous Recombination. Mol Cell. 2017 Jun 1;66(5):622-634.e8. PMID: 28575658
35. Antoniuk-Majchrzak J, Enkhbaatar T, Długajczyk A, Kaminska J, Skoneczny M, Klionsky DJ, et al. Stability of Rad51 recombinase and persistence of Rad51 DNA repair foci depends on post-translational modifiers, ubiquitin and SUMO. Biochim Biophys Acta Mol Cell Res. 2023 Oct;1870(7):119526. PMID: 37364618
36. Zhang J, Ma Z, Treszezamsky A, Powell SN. MDC1 interacts with Rad51 and facilitates homologous recombination. Nat Struct Mol Biol. 2005 Oct;12(10):902–909. PMID: 16186822

37. Cruz C, Castroviejo-Bermejo M, Gutiérrez-Enríquez S, Llop-Guevara A, Ibrahim YH, Gris-Oliver A, et al. RAD51 foci as a functional biomarker of homologous recombination repair and PARP inhibitor resistance in germline BRCA-mutated breast cancer. Ann Oncol. 2018 May 1;29(5):1203–1210. PMCID: PMC5961353
38. Certo MT, Ryu BY, Annis JE, Garibov M, Jarjour J, Rawlings DJ, et al. Tracking genome engineering outcome at individual DNA breakpoints. Nat Methods. 2011 Jul 10;8(8):671–676. PMCID: PMC3415300
39. Dodson AE, Shenker S, Sullivan P, Nayak SU, Middleton C, McGuire M, et al. Pan-cancer Analysis of Homologous Recombination Deficiency in Cell Lines. Cancer Res Commun. 2024 Nov 1; PMID: 39485057
40. Knijnenburg TA, Wang L, Zimmermann MT, Chambwe N, Gao GF, Cherniack AD, et al. Genomic and Molecular Landscape of DNA Damage Repair Deficiency across The Cancer Genome Atlas. Cell Rep. 2018 Apr 3;23(1):239-254.e6. PMCID: PMC5961503
41. Timms KM, Abkevich V, Hughes E, Neff C, Reid J, Morris B, et al. Association of BRCA1/2 defects with genomic scores predictive of DNA damage repair deficiency among breast cancer subtypes. Breast Cancer Res BCR. 2014 Dec 5;16(6):475. PMCID: PMC4308910
42. Birkbak NJ, Wang ZC, Kim JY, Eklund AC, Li Q, Tian R, et al. Telomeric allelic imbalance indicates defective DNA repair and sensitivity to DNA-damaging agents. Cancer Discov. 2012 Apr;2(4):366–375. PMCID: PMC3806629
43. Popova T, Manié E, Rieunier G, Caux-Moncoutier V, Tirapo C, Dubois T, et al. Ploidy and large-scale genomic instability consistently identify basal-like breast carcinomas with BRCA1/2 inactivation. Cancer Res. 2012 Nov 1;72(21):5454–5462. PMID: 22933060
44. Abkevich V, Timms KM, Hennessy BT, Potter J, Carey MS, Meyer LA, et al. Patterns of genomic loss of heterozygosity predict homologous recombination repair defects in epithelial ovarian cancer. Br J Cancer. 2012 Nov 6;107(10):1776–1782. PMCID: PMC3493866
45. Daemen A, Wolf DM, Korkola JE, Griffith OL, Frankum JR, Brough R, et al. Cross-platform pathway-based analysis identifies markers of response to the PARP inhibitor olaparib. Breast Cancer Res Treat. 2012 Sep;135(2):505–517. PMCID: PMC3429780
46. Wolf DM, Yau C, Sanil A, Glas A, Petricoin E, Wulfkuhle J, et al. DNA repair deficiency biomarkers and the 70-gene ultra-high risk signature as predictors of veliparib/carboplatin response in the I-SPY 2 breast cancer trial. NPJ Breast Cancer. 2017;3:31. PMCID: PMC5572474
47. Pusztai L, Yau C, Wolf DM, Han HS, Du L, Wallace AM, et al. Durvalumab with olaparib and paclitaxel for high-risk HER2-negative stage II/III breast cancer: Results from the adaptively randomized I-SPY2 trial. Cancer Cell. 2021 Jul 12;39(7):989-998.e5. PMCID: PMC11064785
48. Moore JA, Chen KT, Madison R, Newberg JY, Fleischmann Z, Wang S, et al. Pan-Cancer Analysis of Copy-Number Features Identifies Recurrent Signatures and a Homologous Recombination Deficiency Biomarker to Predict Poly (ADP-Ribose) Polymerase Inhibitor Response. JCO Precis Oncol. 2023 Sep;7:e2300093. PMID: 37769224
49. Cortesi L, Rugo HS, Jackisch C. An Overview of PARP Inhibitors for the Treatment of Breast Cancer. Target Oncol. 2021 May;16(3):255–282. PMCID: PMC8105250
50. Sikora MJ, Jacobsen BM, Levine K, Chen J, Davidson NE, Lee AV, et al. WNT4 mediates estrogen receptor signaling and endocrine resistance in invasive lobular carcinoma cell lines. Breast Cancer Res BCR. 2016 Sep 20;18(1):92. PMCID: PMC5028957
51. Du T, Sikora MJ, Levine KM, Tasdemir N, Riggins RB, Wendell SG, et al. Key regulators of lipid metabolism drive endocrine resistance in invasive lobular breast cancer. Breast Cancer Res BCR. 2018 Sep 4;20(1):106. PMCID: PMC6124012
52. Sikora MJ, Cooper KL, Bahreini A, Luthra S, Wang G, Chandran UR, et al. Invasive lobular carcinoma cell lines are characterized by unique estrogen-mediated gene expression patterns and altered tamoxifen response. Cancer Res. 2014 Mar 1;74(5):1463–1474. PMCID: PMC3955299
53. Scherer SD, Riggio AI, Haroun F, DeRose YS, Ekiz HA, Fujita M, et al. An immune-humanized patient-derived xenograft model of estrogen-independent, hormone receptor positive metastatic breast cancer. Breast Cancer Res BCR. 2021 Oct 30;23(1):100. PMCID: PMC8556932

54. Thomas M, Kelly ED, Abraham J, Kruse M. Invasive lobular breast cancer: A review of pathogenesis, diagnosis, management, and future directions of early stage disease. Semin Oncol. 2019 Apr;46(2):121–132. PMID: 31239068
55. Rempel E, Kluck K, Beck S, Ourailidis I, Kazdal D, Neumann O, et al. Pan-cancer analysis of genomic scar patterns caused by homologous repair deficiency (HRD). NPJ Precis Oncol. 2022 Jun 9;6(1):36. PMCID: PMC9184602
56. Pareja F, Ferrando L, Lee SSK, Beca F, Selenica P, Brown DN, et al. The genomic landscape of metastatic histologic special types of invasive breast cancer. Npj Breast Cancer. Nature Publishing Group; 2020 Oct 14;6(1):1–10.
57. Sammons S, Raskina K, Danziger N, Alder L, Schrock AB, Venstrom JM, et al. APOBEC Mutational Signatures in Hormone Receptor-Positive Human Epidermal Growth Factor Receptor 2-Negative Breast Cancers Are Associated With Poor Outcomes on CDK4/6 Inhibitors and Endocrine Therapy. JCO Precis Oncol. 2022 Oct;6:e2200149. PMCID: PMC9666120
58. Gupta A, Gazzo A, Selenica P, Safonov A, Pareja F, Silva EM da, et al. APOBEC3 mutagenesis drives therapy resistance in breast cancer. bioRxiv. 2024 May 1;2024.04.29.591453.
59. Shen B, Chapman JH, Custance MF, Tricola GM, Jones CE, Furano AV. Perturbation of base excision repair sensitizes breast cancer cells to APOBEC3 deaminase-mediated mutations. eLife. 2020 Jan 6;9:e51605. PMCID: PMC6961979
60. Venkatesan S, Rosenthal R, Kanu N, McGranahan N, Bartek J, Quezada SA, et al. Perspective: APOBEC mutagenesis in drug resistance and immune escape in HIV and cancer evolution. Ann Oncol Off J Eur Soc Med Oncol. 2018 Mar 1;29(3):563–572. PMCID: PMC5888943
61. Litton JK, Rugo HS, Ettl J, Hurvitz SA, Gonçalves A, Lee KH, et al. Talazoparib in Patients with Advanced Breast Cancer and a Germline BRCA Mutation. N Engl J Med. 2018 Aug 23;379(8):753–763. PMCID: PMC10600918
62. Turner NC, Telli ML, Rugo HS, Mailliez A, Ettl J, Grischke EM, et al. A Phase II Study of Talazoparib after Platinum or Cytotoxic Nonplatinum Regimens in Patients with Advanced Breast Cancer and Germline BRCA1/2 Mutations (ABRAZO). Clin Cancer Res. 2019 May 1;25(9):2717–2724. PMID: 30563931
63. Litton JK, Scoggins ME, Hess KR, Adrada BE, Murthy RK, Damodaran S, et al. Neoadjuvant Talazoparib for Patients With Operable Breast Cancer With a Germline BRCA Pathogenic Variant. J Clin Oncol. 2020 Feb 10;38(5):388–394. PMCID: PMC7351336
64. Litton JK, Beck JT, Jones JM, Andersen J, Blum JL, Mina LA, et al. Neoadjuvant Talazoparib in Patients With Germline BRCA1/2 Mutation-Positive, Early-Stage Triple-Negative Breast Cancer: Results of a Phase II Study. The Oncologist. 2023 Oct 3;28(10):845–855. PMCID: PMC10546823
65. Sflomos G, Schipper K, Koorman T, Fitzpatrick A, Oesterreich S, Lee AV, et al. Atlas of Lobular Breast Cancer Models: Challenges and Strategic Directions. Cancers. 2021 Oct 27;13(21):5396. PMCID: PMC8582475
66. Bahnassy S, Sikora MJ, Riggins RB. Unlocking the Mysteries of Lobular Breast Cancer Biology Needs the Right Combination of Preclinical Models. Mol Cancer Res MCR. 2022 Jun 3;20(6):837–840. PMID: 35276005
67. Shah OS, Chen F, Wedn A, Kashiparekh A, Knapick B, Chen J, et al. Multi-omic characterization of ILC and ILC-like cell lines as part of ILC cell line encyclopedia (ICLE) defines new models to study potential biomarkers and explore therapeutic opportunities. BioRxiv Prepr Serv Biol. 2023 Dec 12;2023.09.26.559548. PMCID: PMC10557671
68. Shackleford MT, Rao DM, Bordeaux EK, Hicks HM, Towers CG, Sottnik JL, et al. Estrogen Regulation of mTOR Signaling and Mitochondrial Function in Invasive Lobular Carcinoma Cell Lines Requires WNT4. Cancers. 2020 Oct 12;12(10):2931. PMCID: PMC7650584
69. Agostinetto E, Nader-Marta G, Paesmans M, Ameye L, Veys I, Buisseret L, et al. ROSALINE: a phase II, neoadjuvant study targeting ROS1 in combination with endocrine therapy in invasive lobular carcinoma of the breast. Future Oncol Lond Engl. 2022 Jul;18(22):2383–2392. PMID: 35695563

70. Voorwerk L, Isaeva OI, Horlings HM, Balduzzi S, Chelushkin M, Bakker NAM, et al. PD-L1 blockade in combination with carboplatin as immune induction in metastatic lobular breast cancer: the GELATO trial. Nat Cancer. 2023 Apr;4(4):535–549. PMCID: PMC10132987
71. McCart Reed AE, Lal S, Kutasovic JR, Wockner L, Robertson A, de Luca XM, et al. LobSig is a multigene predictor of outcome in invasive lobular carcinoma. NPJ Breast Cancer. 2019;5:18. PMCID: PMC6597578
72. Sflomos G, Battista L, Aouad P, De Martino F, Scabia V, Stravodimou A, et al. Intraductal xenografts show lobular carcinoma cells rely on their own extracellular matrix and LOXL1. EMBO Mol Med. 2021 Mar 5;13(3):e13180. PMCID: PMC7933935
73. Olukoya AO, Stires H, Bahnassy S, Persaud S, Guerra Y, Ranjit S, et al. Riluzole Suppresses Growth and Enhances Response to Endocrine Therapy in ER+ Breast Cancer. J Endocr Soc. 2023 Aug 28;7(10):bvad117. PMCID: PMC10521904
74. Van Baelen K, Geukens T, Maetens M, Tjan-Heijnen V, Lord CJ, Linn S, et al. Current and future diagnostic and treatment strategies for patients with invasive lobular breast cancer. Ann Oncol. 2022 Aug;33(8):769–785. PMID: 35605746
75. Xie Z, Bailey A, Kuleshov MV, Clarke DJB, Evangelista JE, Jenkins SL, et al. Gene Set Knowledge Discovery with Enrichr. Curr Protoc. 2021 Mar;1(3):e90. PMCID: PMC8152575
76. Sikora MJ, Johnson MD, Lee AV, Oesterreich S. Endocrine Response Phenotypes Are Altered by Charcoal-Stripped Serum Variability. Endocrinology. 2016 Oct;157(10):3760–3766. PMCID: PMC5045515
77. Cerami E, Gao J, Dogrusoz U, Gross BE, Sumer SO, Aksoy BA, et al. The cBio cancer genomics portal: an open platform for exploring multidimensional cancer genomics data. Cancer Discov. 2012 May;2(5):401–404. PMCID: PMC3956037
78. Stirling DR, Swain-Bowden MJ, Lucas AM, Carpenter AE, Cimini BA, Goodman A. CellProfiler 4: improvements in speed, utility and usability. BMC Bioinformatics. 2021 Sep 10;22(1):433. PMCID: PMC8431850
79. Rao DM, Shackleford MT, Bordeaux EK, Sottnik JL, Ferguson RL, Yamamoto TM, et al. Wnt family member 4 (WNT4) and WNT3A activate cell-autonomous Wnt signaling independent of porcupine O-acyltransferase or Wnt secretion. J Biol Chem. 2019 Dec 27;294(52):19950–19966. PMCID: PMC6937561

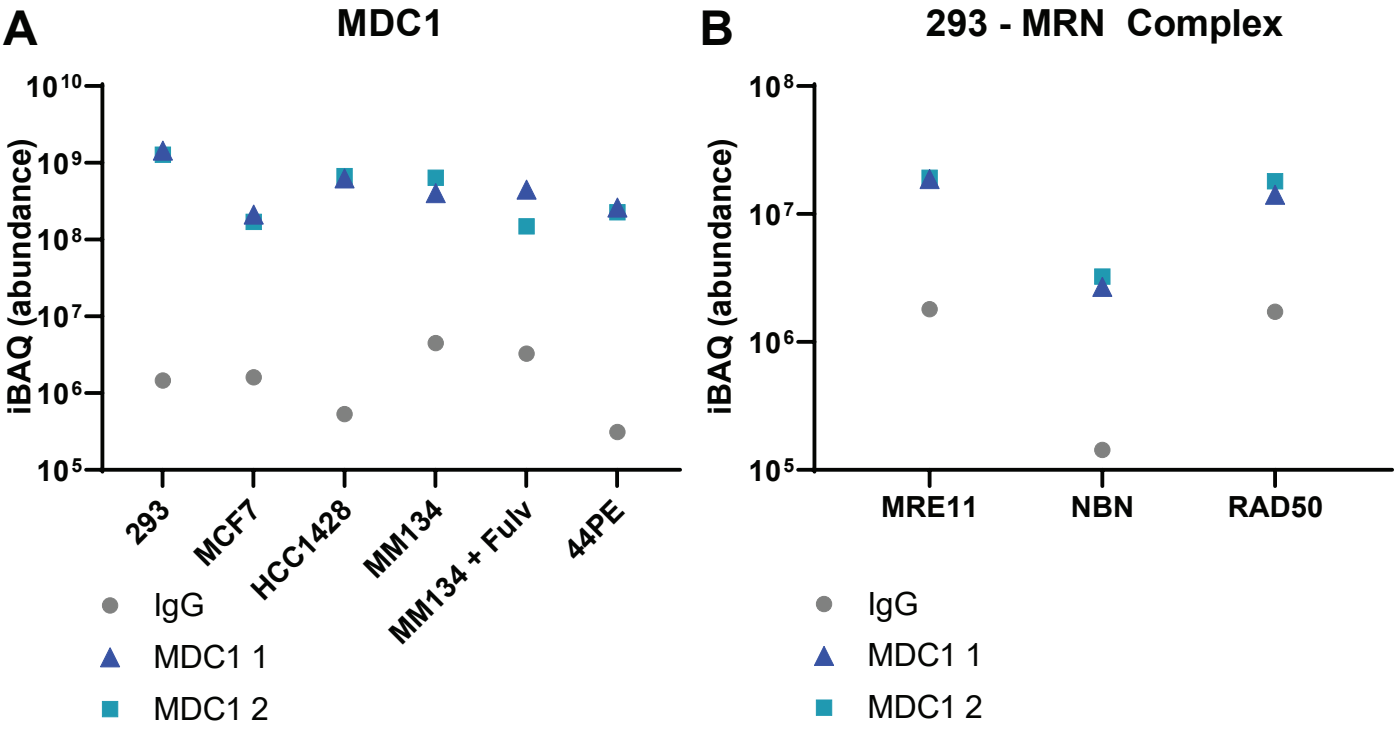

C 293 - Enriched Pathways (GO Biological Processes)

Term	Overlap	adj.p
DNA metabolic process (GO:0006259)	68/277	9.06E-20
transcription, DNA-templated (GO:0006351)	58/221	2.35E-18
DNA repair (GO:0006281)	68/298	2.46E-18
chromatin remodeling (GO:0006338)	36/103	2.18E-15
transcription elongation from RNA polymerase II promoter (GO:0006368)	29/67	3.74E-15
transcription by RNA polymerase II (GO:0006366)	65/320	5.73E-15
DNA-templated transcription, elongation (GO:0006354)	29/69	7.13E-15
cellular response to DNA damage stimulus (GO:0006974)	68/350	8.62E-15
negative regulation of cellular macromolecule biosynthetic process (GO:2000113)	88/547	3.71E-14
ATP-dependent chromatin remodeling (GO:0043044)	22/42	1.20E-13

DNA repair (GO:0006281)

MDC1	BLM
FEN1	VCP
SETD2	PRKDC
TRRAP	DOT1L
MPG	IGHMBP2
CETN2	XPC
NUCKS1	BRCC3
HERC2	PDS5A
TRIM28	MTA1
NBN	RAD21
KPNA2	POLD1
MEN1	NSD2
PIAS4	ASCC2
RFC5	ASCC3
UPF1	FANCI
RFC4	NPM1
PARP1	XRCC5
PARP2	INTS3
RFC2	SMARCA5
LIG3	RPA1
WRNIP1	HMGA2
CSNK1E	GTF2H1
CHD1L	GTF2H3
ACTR8	APTX
BAZ1B	GTF2H4
SMC1A	GTF2H5
RAD23B	RAD50
INIP	ERCC3
REXO4	RPA3
DDB1	ERCC2
MSH6	CDK1
MSH2	TRIP13
MSH3	MNAT1
TP53	NOP53

ATP-dependent chromatin remodeling (GO:0043044)

MBD3
SMARCE1
HDAC2
SMARCD2
PBRM1
SMARCC1
SMARCB1
HDAC1
CHD8
MBD2
SMARCA5
CHD4
CHD3
ACTR8
SMARCA1
ARID1B
SMARCA2
ACTB
GATAD2B
SMARCA4
SMARCAD1
MTA2

Supplemental Figure 1. MDC1 is strongly enriched in IP/MS and key DNA repair partners are identified in 293 cells. (A) iBAQ abundance values for MDC1 peptides for biological duplicate MDC1 IP and IgG controls. **(B)** iBAQ abundance values from 293 cells, for MRN complex proteins as positive control for identifying previously reported constitutive MDC1 partners in 293 cells. **(C)** Gene set enrichment against GO Biological Processes, with identified proteins in two highlighted pathways at right.

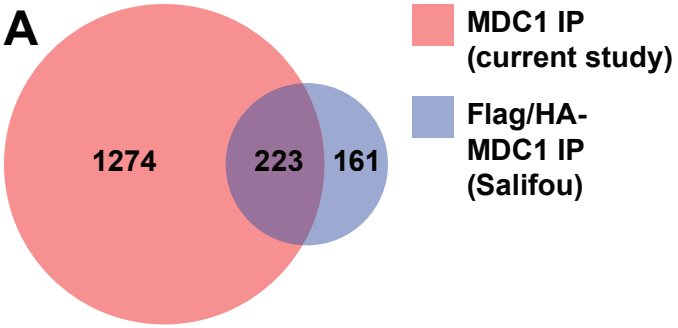

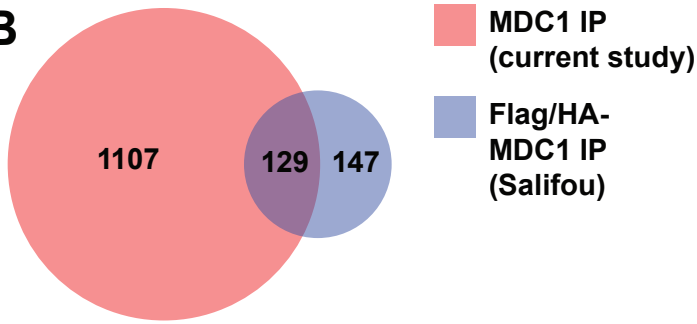

Unfiltered: GO-Biological Processes

MDC1 IP specific	adj.p
1 ribosome biogenesis (GO:0042254)	2.97E-58
2 ncRNA processing (GO:0034470)	3.23E-56
3 rRNA processing (GO:0006364)	2.44E-54
4 rRNA metabolic process (GO:0016072)	2.70E-50
5 gene expression (GO:0010467)	8.94E-34
6 mRNA processing (GO:0006397)	1.53E-28
Shared	
1 RNA splicing, via transesterification reactions with bulged adenosine as nucleophile (GO:0000377)	3.26E-54
2 mRNA splicing, via spliceosome (GO:0000398)	2.22E-52
3 gene expression (GO:0010467)	2.22E-52
4 mRNA processing (GO:0006397)	3.77E-50
nuclear-transcribed mRNA catabolic process,	
5 nonsense-mediated decay (GO:0000184)	1.08E-45
6 cytoplasmic translation (GO:0002181)	1.94E-42
Flag/HA-MDC1 IP specific	
1 mRNA splicing, via spliceosome (GO:0000398)	6.31E-13
2 RNA splicing, via transesterification […] (GO:0000377)	8.44E-12
3 mRNA processing (GO:0006397)	1.63E-10
anaphase-promoting complex-dependent	
4 catabolic process (GO:0031145)	4.02E-07
5 regulation of cell cycle phase transition (GO:1901987)	1.09E-06
6 proteasomal ubiquitin-independent protein catabolic process (GO:0010499)	3.12E-06

Filtered: GO-Biological Processes

MDC1 IP specific	adj.p
1 transcription, DNA-templated (GO:0006351)	2.45E-14
2 transcription elongation from RNA polymerase II promoter (GO:0006368)	5.43E-14
3 chromatin remodeling (GO:0006338)	5.43E-14
4 DNA metabolic process (GO:0006259)	6.87E-14
5 DNA-templated transcription, elongation (GO:0006354)	6.99E-14
6 DNA repair (GO:0006281)	7.38E-14
Shared	
1 metaphase/anaphase transition of cell cycle (GO:0044784)	4.21E-08
2 metaphase/anaphase transition of mitotic cell cycle (GO:0007091)	4.21E-08
3 positive regulation of metaphase/anaphase transition of cell cycle (GO:1902101)	2.15E-06
4 positive regulation of mitotic metaphase/anaphase transition (GO:0045842)	2.15E-06
5 positive regulation of mitotic sister chromatid separation (GO:1901970)	2.15E-06
6 regulation of cell cycle phase transition (GO:1901987)	2.44E-06
Flag/HA-MDC1 IP specific	
1 anaphase-promoting complex-dependent catabolic process (GO:0031145)	6.48E-07
2 regulation of cell cycle phase transition (GO:1901987)	1.11E-06
3 proteasomal ubiquitin-independent protein catabolic process (GO:0010499)	3.55E-06
4 gluconeogenesis (GO:0006094)	5.06E-06
5 hexose biosynthetic process (GO:0019319)	6.78E-06
6 regulation of mitotic cell cycle (GO:0007346)	1.56E-05

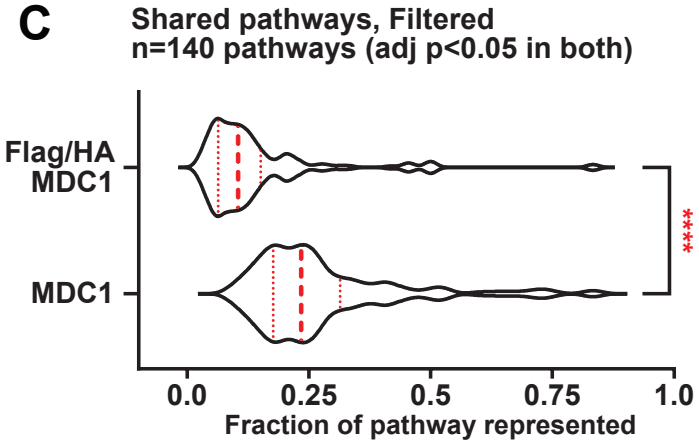

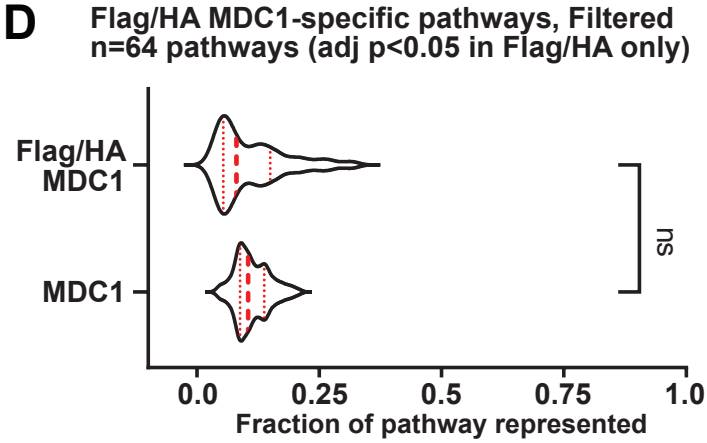

Supplemental Figure 2. MDC1 IP/MS with specific antibody provided greater depth in pathway coverage and new target compared to affinity tag IP/MS. (A-B) Comparing 293 MDC1 IP/MS versus hits reported by Salifou et al (see text). **(A)** Gene set enrichment against GO Biological Processes, without filtering hits from RNA metabolic pathways, from study-specific versus shared MS hits. **(B)** Gene set enrichment against GO Biological Processes, after filtering hits from RNA metabolic pathways. DNA repair and associated pathways were among the top hits only from MDC1 antibody IP/MS. **(C)** MDC1 IP/MS provided greater pathway coverage among GO BP pathways enriched in both IP/MS studies. ****, t-test, $p<0.0001$. **(D)** For pathways that were enriched specifically in Salifou et al affinity tag IP/MS, MDC1 IP/MS provided equivalent pathway coverage in identified peptides.

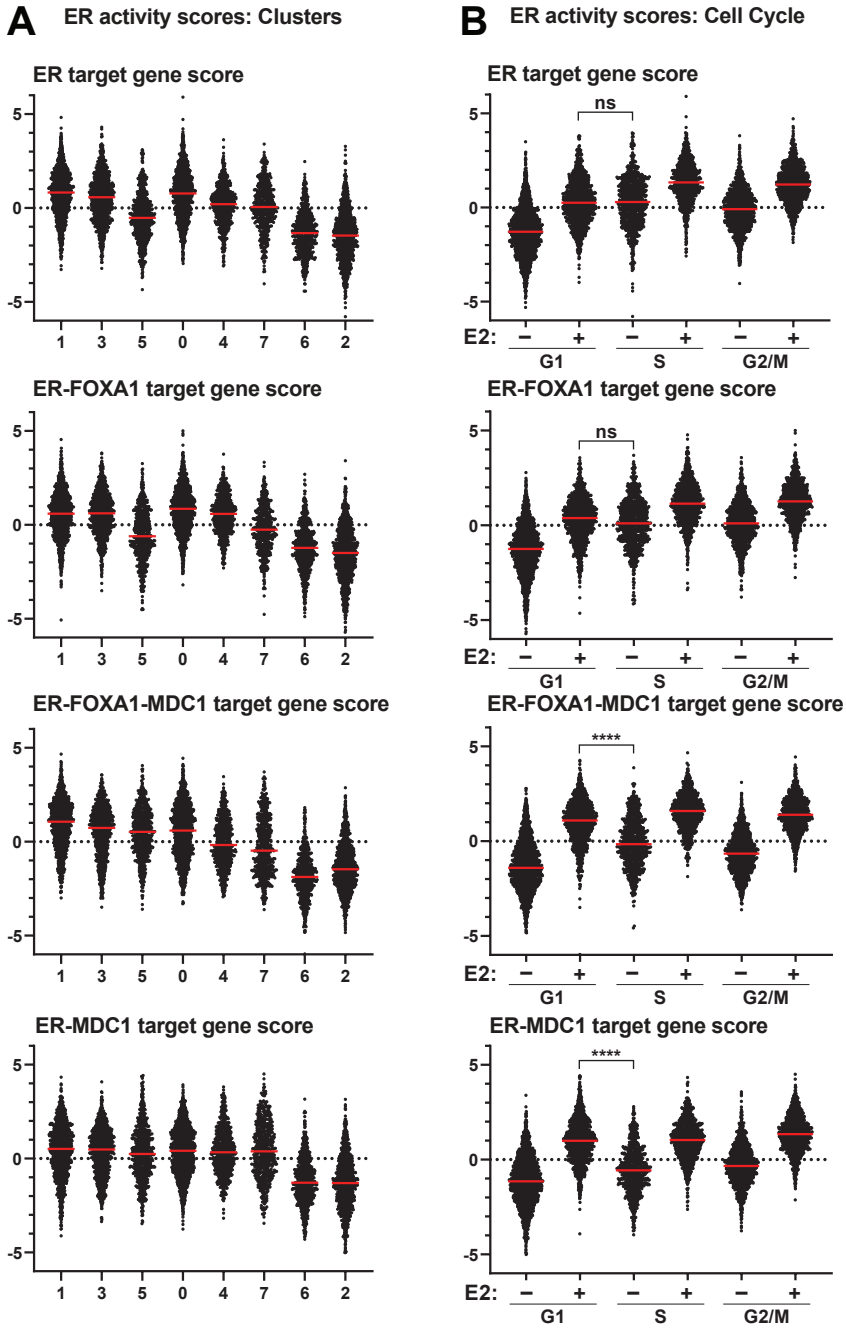

Supplemental Figure 3. ER target gene sets and FOXA1 vs MDC1 activity are distinct across gene expression clusters, cell cycle status, and treatment group. (A) Single cell data represented by the heatmap in Figure 3C, red line = median score, points = individual cells. **(B)** ER target gene set scores by treatment (±E2) and predicted cell cycle state. Comparison between G1/+E2 and S/–E2 is representative of the cell cycle-dependent increase in non-MDC1 target genes (ER, ER-FOXA1 targets) compared to MDC1 target genes (ER-FOXA1-MDC1, ER-MDC1); i.e. for the former, target gene scores are increased in S/G2 relative to G1 regardless of estrogen treatment. ****, ANOVA, adj.p <0.0001.

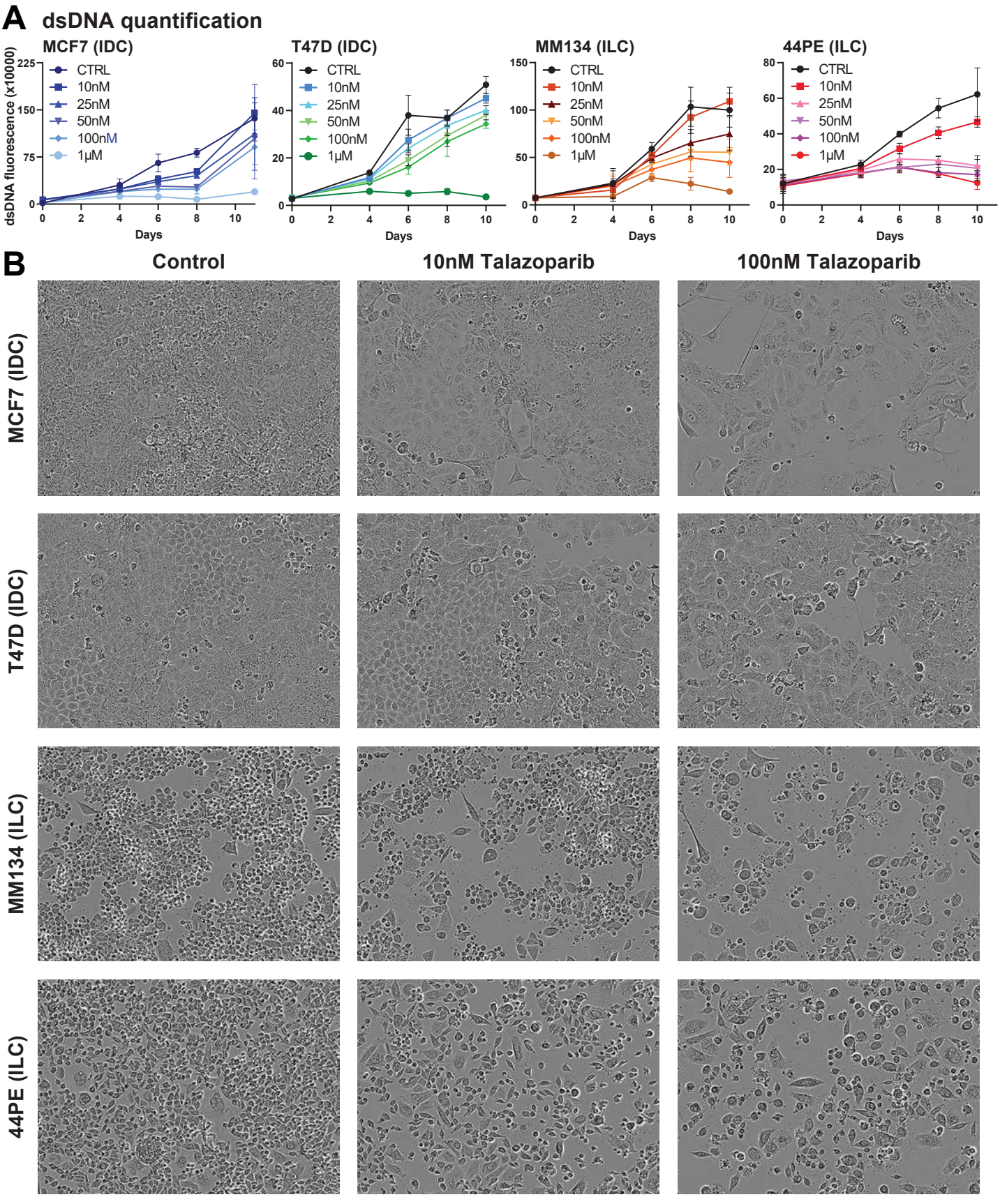

Supplemental Figure 4. ILC cells are sensitive to PARPi talazoparib *in vitro*. (A) Time course of cell proliferation, assessed by dsDNA quantification, with increasing concentration of talazoparib. Extended >7d suggest decreased long-term viability in ILC cells specifically after the single talazoparib treatment. **(B)** Representative Incucyte images after 9 days of treatment as indicated. Remaining IDC cells are fewer than control but morphologically appear healthy and viable, whereas ILC cells show irregular morphology consistent with apoptosis or other cell death.

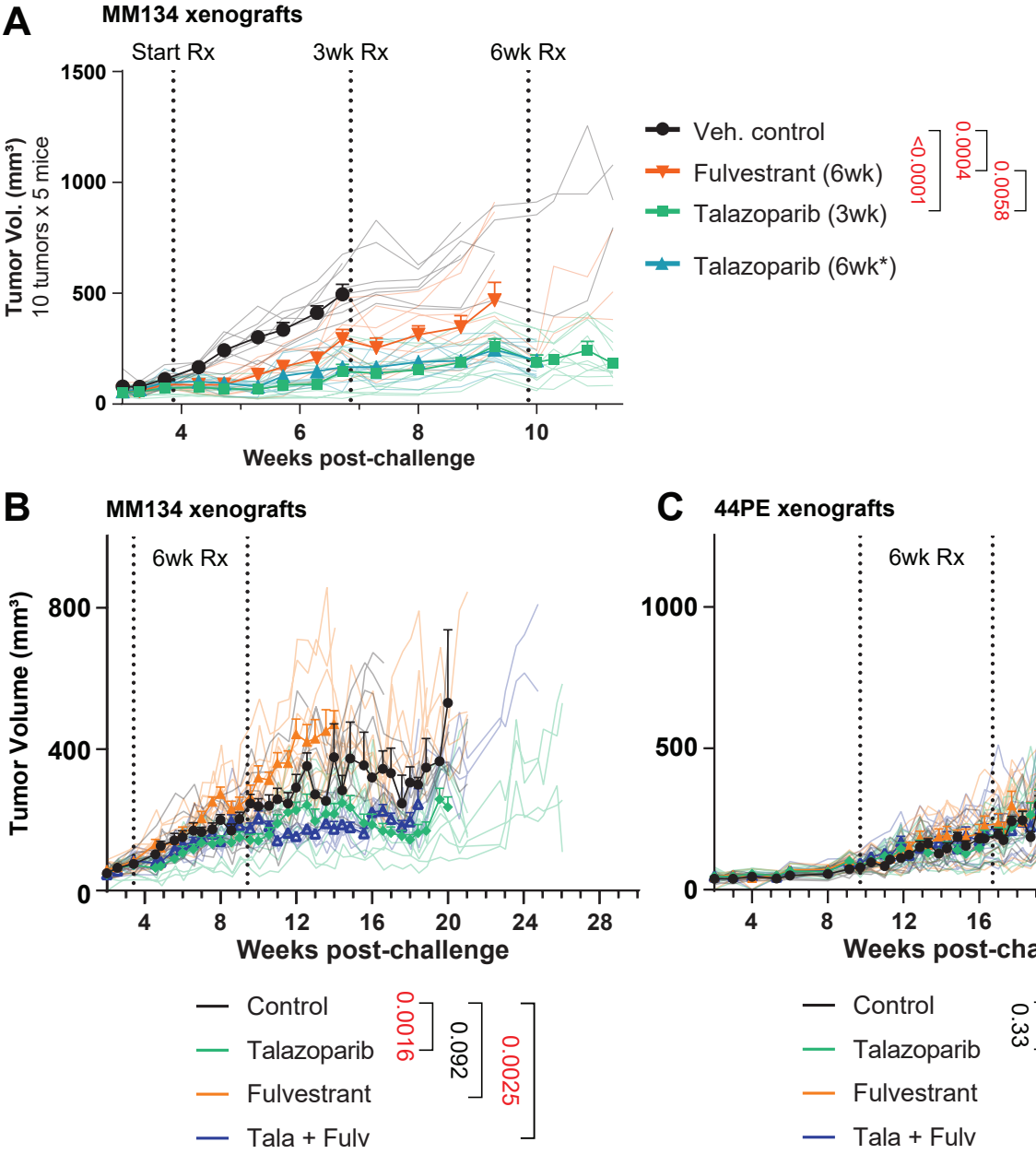

Supplemental Figure 5. ILC cells are sensitive to PARPi talazoparib *in vivo*. Bold lines/symbols show mean tumor size ± SEM; individual tumor size shown as matching faded lines. Bold lines ended at first tumor size human endpoint reached per arm. Two-way ANOVA treatment effect p-values shown. **(A)** 6wk talazoparib data excluded from statistical analyses. **(B-C)** Control and Talazoparib arms also shown in Figure 7.